



2024


A quick and cost-effective method for monitoring deforestation of oil sands mining activities using Synthetic Aperture Radar and Multispectral real-time satellite data from Sentinel-1 and Sentinel-2.

Author(s) ORCID Identifier:

 Jose Garcia-del-Real:  0000-0002-7812-7314

Manuel Alcaraz:  0000-0002-5982-8983

Follow this and additional works at: <https://jsm.gig.eu/journal-of-sustainable-mining>

 Part of the [Explosives Engineering Commons](#), [Oil, Gas, and Energy Commons](#), and the [Sustainability Commons](#)

Recommended Citation

Garcia del Real, J and Alcaraz, M. (2024) "A quick and cost-effective method for monitoring deforestation of oil sands mining activities using Synthetic Aperture Radar and Multispectral real-time satellite data from Sentinel-1 and Sentinel-2.," *Journal of Sustainable Mining*. Vol. 23 : Iss. 1 , Article 8.
Available at: <https://doi.org/10.46873/2300-3960.1403>

This Research Article is brought to you for free and open access by Journal of Sustainable Mining. It has been accepted for inclusion in Journal of Sustainable Mining by an authorized editor of Journal of Sustainable Mining.

A quick and cost-effective method for monitoring deforestation of oil sands mining activities using Synthetic Aperture Radar and Multispectral real-time satellite data from Sentinel-1 and Sentinel-2.

Abstract

Alberta's oil sands mining operations rank among the largest human-made structures globally. Monitoring through the use of Synthetic Aperture Radar (SAR) and Multispectral satellite imaging is an indispensable strategy in attaining sustainable development and mitigating deforestation in the third-largest verified oil reserves worldwide. This paper introduces a novel approach for cost-effective and reliable monitoring of deforestation caused by oil sands mining, avoiding cumbersome methods. It focuses on observing forest/non-forest areas affected by Suncor Energy Company's mining assets in Alberta, using a combination of SAR and Multispectral satellite remote sensing. Radar images from Sentinel-1B and Multispectral images from Sentinel-2A were analyzed with SNAP 8.0 and QGIS within a time series from June 2017 to June 2020, providing detailed information to monitor better the potential environmental impact of oil sands mining activities in Canada. The Sentinel satellite system offers several advantages, including near-global coverage, elevated spatial resolution for detecting small-scale deforestation instances, and the ability to track temporal and dynamic changes through time-series analysis. Additionally, the system's open data policy promotes accessibility, collaboration among researchers, and innovative deforestation monitoring applications. The research results hold potential value for decision-makers, enhancing the efficiency and sustainable development of Suncor's mining operations.

Keywords

Oil sands, Synthetic aperture radar, Multispectral remote sensing, Deforestation, Sustainable development

Creative Commons License



This work is licensed under a [Creative Commons Attribution-NonCommercial-No Derivative Works 4.0 License](https://creativecommons.org/licenses/by-nc-nd/4.0/).

A quick and cost-effective method for monitoring deforestation of oil sands mining activities using synthetic aperture radar and multispectral real-time satellite data from Sentinel-1 and Sentinel-2

J. Garcia-del-Real*, M. Alcaraz

Polytechnic University of Cartagena, Mining and Civil Engineering, Cartagena, Spain

Abstract

Alberta's oil sands mining operations rank among the largest human-made structures globally. Monitoring through the use of Synthetic Aperture Radar (SAR) and Multispectral satellite imaging is an indispensable strategy in attaining sustainable development and mitigating deforestation in the third-largest verified oil reserves worldwide. This paper introduces a novel approach for cost-effective and reliable monitoring of deforestation caused by oil sands mining, avoiding cumbersome methods. It focuses on observing forest/non-forest areas affected by Suncor Energy Company's mining assets in Alberta, using a combination of SAR and Multispectral satellite remote sensing. Radar images from Sentinel-1B and Multispectral images from Sentinel-2A were analyzed with SNAP 8.0 and QGIS within a time series from June 2017 to June 2020, providing detailed information to monitor better the potential environmental impact of oil sands mining activities in Canada. The Sentinel satellite system offers several advantages, including near-global coverage, elevated spatial resolution for detecting small-scale deforestation instances, and the ability to track temporal and dynamic changes through time-series analysis. Additionally, the system's open data policy promotes accessibility, collaboration among researchers, and innovative deforestation monitoring applications. The research results hold potential value for decision-makers, enhancing the efficiency and sustainable development of Suncor's mining operations.

Keywords: Oil sands, Synthetic aperture radar, Multispectral remote sensing, Deforestation, Sustainable development

1. Introduction

Remote sensing technology has been used in the oil sands industry in Canada for several decades. The oil sands, also known as tar sands, are a type of unconventional oil deposit that is found primarily in the province of Alberta. These deposits are a mixture of sand, clay, water, and bitumen, a heavy and viscous form of oil [1].

The oil sands industry in Canada is one of the largest in the world, and the use of remote sensing technology has been critical in its development. Remote sensing technology has been used to map the extent and distribution of the oil sands deposits, as well as to monitor the environmental impacts of oil sands development [2]. Early applications of remote sensing in the oil sands included the use of

aerial photography and satellite imagery to map the surface features of the oil sands deposits. This allowed for the identification of areas that were suitable for mining and extraction.

In recent years, the use of remote sensing technology in the oil sands has expanded to include the use of satellite-based sensors, such as radar and lidar, to map the subsurface geology of the oil sands deposits [3]. This has helped to improve the accuracy of resource estimates and to optimize the design of mining and extraction operations. This technology has also been used to monitor the environmental impacts of oil sands development, such as the rate of vegetation loss, land surface changes, and water quality [4].

In this line, deforestation is one of the most significant environmental issues facing our planet

Received 5 February 2023; revised 20 July 2023; accepted 26 July 2023.
Available online 11 January 2024

* Corresponding author.
E-mail address: jg6377731@gmail.com (J. Garcia-del-Real).

<https://doi.org/10.46873/2300-3960.1403>
2300-3960/© Central Mining Institute, Katowice, Poland. This is an open-access article under the CC-BY 4.0 license
(<https://creativecommons.org/licenses/by/4.0/>).

today [5], and it has a wide range of negative impacts on biodiversity, climate change, and human populations [6]. According to some authors, the oil sands mining industry could be considered a major contributor to deforestation, as it requires the removal of large areas of forest for mining activities [7,8]. Traditional methods for monitoring deforestation in the oil sands mining region are costly and time-consuming, making it difficult to accurately measure and track the extent of deforestation [9].

Synthetic Aperture Radar (SAR) and multispectral satellite data have proven to be effective tools for monitoring deforestation in other regions [10]. SAR uses radar waves to penetrate through clouds and vegetation, providing detailed information about the forest canopy and the underlying soil [11]. Multispectral satellite data, on the other hand, provides information about the reflectance of different parts of the electromagnetic spectrum, which can be used to identify the different types of vegetation and land cover [12].

However, it is well-known that multispectral imagery technology may have some limitations depending on the cloud coverage since, for instance, clouds can block the view of the earth's surface, making it difficult to obtain data in certain areas and pushing researchers to develop different techniques to remove their negative effects [13,14]. Another limitation is the Atmospheric Correction since acquiring accurate information from multispectral imagery requires correction for atmospheric effects, such as absorption and scattering of light. These corrections are complex and require knowledge of the atmospheric conditions at the time of data acquisition [15,16].

Therefore, Synthetic Aperture Radar (SAR) and Multispectral real-time satellite data have a high potential to monitor deforestation caused by oil sands mining activities. SAR uses radar to create detailed images of the earth's surface, even through cloud cover and darkness and can be useful to detect changes in the landscape, such as deforestation. Multispectral data, on the other hand, uses different wavelengths of light to capture information about the earth's surface and can be used to identify specific types of vegetation, such as trees. Together, SAR and multispectral data are key to monitoring the extent and rate of deforestation caused by oil sands mining activities, providing valuable information for conservation efforts and sustainable resource management.

On the other hand, the Multispectral data of Sentinel-2 is, in this sense, notably advantageous. Since it provides additional information, as for instance, vegetation indices and land cover

classification [17], which can be key not only for differentiating deforested regions but also for the identification of diverse land cover types [18] and the evaluation of the environmental implications of mining activities. By merging SAR and Multispectral data, a comprehensive perspective of the deforestation procedure is presented.

In addition to the innovations and novelties mentioned before in the field of environmental monitoring, Sentinel 1 and Sentinel 2 provide near-global coverage and regular imaging, allowing for the monitoring of deforestation in remote and vast areas. Hence, it is recommendable for oil sands mining sites. This comprehensive coverage ensures no significant changes go unnoticed, enabling timely intervention and assessment. Furthermore, due to their high spatial resolution imagery, the combined use of both satellites allows the detection and monitoring of other types of small-scale deforestation activities [19]. On top of that, it is worth noting the change detection capability to capture temporal changes, which enables the detection of deforestation events over time. For instance, by utilizing time-series analysis techniques, such as interferometry or coherence analysis, it becomes possible to monitor the progression and expansion of deforestation activities associated with oil sands mining activities.

Another important aspect that should be emphasized in this regard, is the enhanced Data accessibility of Sentinel 1 and Sentinel 2. The open data policy of the Sentinel satellites ensures free and open access to SAR and Multispectral data, which could be key to democratizing the availability of monitoring tools [20], [21]. Moreover, this enhanced accessibility fosters collaboration among researchers, facilitates scientific research, and paves the way for the development of innovative applications for deforestation monitoring.

A review of the literature found that the combination of SAR and multispectral satellite data has the potential to provide a quick and cost-effective method for monitoring deforestation [22] in the oil sands mining region in almost all weather conditions. Moreover, by using real-time satellite data, it is possible to track changes in the forest canopy in near real-time, providing valuable information for decision-makers and conservationists.

Some investigations have evidenced the efficacy of said methodologies in identifying and measuring forest disruptions such as selective logging and deforestation. For example, a new approach using spaceborne SAR interferometry has been developed to detect and quantify selective logging events, providing accurate monitoring of height changes

due to forest growth and degradation [23]. Additionally, a time-series model has been proposed to characterize land cover change, reconstructing the underlying continuous land change process from satellite observations and deriving the timing, intensity, and duration of deforestation [24]. Furthermore, for instance, a novel multispectral time series change monitoring method combining dimension reduction methods with a sequential hypothesis test automatically selects a suitable index for deforestation monitoring and improves accuracy in the presence of strong seasonality [25]. These studies highlight the potential of time-series analysis techniques for monitoring deforestation activities.

Another important aspect worth mentioning in relation to surface soil moisture content and porosity of deposits is the fact that Sentinel-1 and Sentinel-2 satellite systems could be utilized to analyze granular and skeletal deposits. In fact, Synthetic Aperture Radar (SAR) data obtained from Sentinel-1 actually provides information on surface roughness [26,27], which is very closely linked to porosity in granular and skeletal deposits. By analyzing, for instance, the distribution and variations of their backscatter intensity values extracted from Sentinel 1 data, which serve as indicator of the strength of the radar signal returned from the surface. Higher values of backscatter intensity are usually associated with rougher surfaces, which may indicate higher porosity in granular and skeletal deposits.

In this sense, Sentinel-2's multispectral data provides additional information about the spectral reflectance of the Earth's surface that, if the reflectance patterns across different spectral bands are duly analyzed, can help to identify the associated variations with the porosity of the different types of deposits. Furthermore, Vegetation indices, such as the Normalized Difference Vegetation Index (NDVI), could be used to indirectly provide insights into a deposit's porosity, for instance, by indicating vegetation cover and health, which usually are aspects related to the presence of porous materials.

The utilization of SAR and multispectral information from both satellites presents an advantageous approach able to obtain the dispersion of surface soil moisture (SSM) and the root mean squared height (RMSH) in bare soils, thus lessening the impact of surface roughness [28]. In this sense, optical and radar data combined can help to improve the accuracy of SSM and RMSH measurements, with decreased root mean squared error and increased retrieval accuracy when compared to using single radar or optical data [29].

Correlation analysis between backscatter intensity derived from SAR data and porosity measurements

could be performed to quantify a potential relationship between each other. The reflectance patterns and vegetation indices obtained from multispectral data have the potential to enhance the SAR analysis by providing supplementary insights about the porosity distribution in the deposits. Field measurements and laboratory analyses of porosity would also be very useful in this regards and could be used to validate the results obtained from satellite data analysis since the combination of both data sources helps to get a better understanding of the porosity characteristics and for validating the data obtained. By doing so, the results could be interpreted to assess the suitability of the granular and skeletal deposits and for various applications, such as for example hydrological studies, construction works, or mineral resource exploration, based on their porosity properties.

Understanding the use of remote sensing technology to monitor these aspects is very important for helping to minimize the environmental footprint of oil sands development and to ensure that the industry operates in an environmentally responsible manner. In fact, the combined use of this technology is crucial as a powerful tool in the exploration, development and management of this important resource. Thus, this research aims to investigate the use of SAR and multispectral satellite data to monitor deforestation in the oil sands mining region, with the ultimate goal of developing a cost-effective and reliable method for monitoring deforestation in this area.

By combining two different approaches (SAR vs. multispectral) for monitoring deforestation of oil sands mining activities in Alberta Province in Canada, the methodology of this study is designed to explore the advantages of using these two remote sensing technologies and focuses its investigation on the mining assets owned by the Suncor Energy company, which is the producer with the biggest reserves of oil tars in Alberta province. Total forest and deforested areas for the time period between June 2017 and June 2020 were efficiently measured. While Vegetation's health was accurately measured, and the Vegetation Spectral Reflectance Curve in different regions of interest (ROIs) within the surrounding areas close to the mining activities was successfully calculated.

It is well proved worldwide the effectiveness of multispectral and SAR technologies for monitoring deforested areas. However, there is little recent literature about its suitability for monitoring oil sands mining activities in Alberta using Sentinel-1 and Sentinel-2 satellite data. Therefore, the study encompasses the measurement of total forest and

deforested areas, assessing vegetation health, for which different tasks were carried out. With respect to the methodology used in this study, it includes a Synthetic Aperture Radar analysis and a supervised Classification Process with a Random Forest algorithm for measuring total forest and deforested areas. After downloading SAR (Sentinel-1B) and multispectral (Sentinel-2A) products, data was pre-processed using software tools like SNAP and its Graph Builder, conducting supervised classification with Random Forest, post-processing data to remove noise, exporting processed products for visualization, and creating time series of deforested areas, and obtaining also the confidence value of classified Sentinel-1B SAR products using SNAP and QGIS. Vegetation's health was measured by calculating the Normalized Difference Vegetation Index (NDVI) and the Vegetation Spectral Reflectance Curve of Sentinel-2A Multispectral optical data for specific regions of interest in SNAP.

Forest and deforested areas were identified accordingly, using images provided by the Sentinel-2A satellite. A multispectral analysis with SNAP and different wavelengths was carried out, utilizing the NIR band (0.7–1.4 μm) and Shortwave Infrared band (1.45 μm , 1.95 μm and 2.5 μm) to check cell structures, water content and leaf biochemical respectively. The Vegetation Spectral Reflectance Curve was calculated for 15 different locations (Pictures 13 and 14) in order to identify “Healthy Green Vegetation” 0.7–1.4 μm , “Stressed Vegetation” 1.4–1.9 μm and “Massive Stressed Vegetation” 1.9–2.5 μm . For checking the health and vitality of vegetation, the Normalized Difference Vegetation Index (NDVI) was calculated, having the most vigorous vegetation within a range value of 0.66–1.0. For NDVI values close to 0.3, it indicated the presence of shrubs and grassland, while NDVI values close to 0.0 corresponded to sand, barren areas of rock, or snow. NDVI values close to -1.0 were related to water areas. Furthermore, a time series analysis over a period of 4 years, from 2017 to 2020, was accomplished successfully.

Finally, this study aims to successfully prove the complementarity among the two proposed technologies, SAR and Multispectral. It opens the door to further and more detailed research by changing, for instance, classification parameters, using also additional operators such as the Grey Level Co-occurrence Matrix (GLCM) for monitoring other areas environmentally or socially affected by oil sand mining exploitations. Research results showed a cost-effective innovative solution based on real-time satellite data for mining and energy companies to improve the decision-making process. It helps them to analyze the

impact of their mining activities and to walk on the path to achieve sustainable development.

2. Materials and methods

2.1. Objectives

1. Measuring total forest and deforested areas for the time period between June 2017 and June 2020, either using data provided by Sentinel-1 and/or Sentinel-2 satellites.
2. Measuring vegetation's health, calculating the Vegetation Spectral Reflectance Curve in different regions of interest (ROIs) within the surrounding areas close to the mining activities.
3. Calculating accuracy on measuring total forest and deforested areas obtained either from Sentinel-1 and/or Sentinel-2 satellite data.

2.2. Tasks

A total of fourteen tasks were carried out in order to meet the three objectives of this study. Description of all tasks successfully accomplished are included in [Table 1](#).

2.3. Research approach

The area of interest was analyzed in order to map the ever-changing forest and provide regular updates on their conditions at a range of spatial and temporal resolutions. Forest and deforested areas were identified accordingly using images provided by Sentinel-1B and Sentinel-2A satellites.

A multispectral analysis with SNAP using different wavelengths was carried out with the data provided by the Sentinel-2A satellite. Utilizing the NIR band (0.7–1.4 μm) and Shortwave Infrared band (1.45 μm , 1.95 μm and 2.5 μm) cell structures, water content and leaf biochemical respectively, could be checked.

The Vegetation Spectral Reflectance Curve was calculated for 15 different regions of interest (ROIs) located within the perimeter of Suncor's mining permits in order to identify “Healthy Green Vegetation” 0.7–1.4 μm , “Stressed Vegetation” 1.4–1.9 μm and “Massive Stressed Vegetation” 1.9–2.5 μm in non-deforested areas. For checking the health and vitality of vegetation, the Normalized Difference Vegetation Index (NDVI) was calculated, using for this purpose a 10-m spatial resolution for the B8 NIR band and B4 RED band centered at 842 nm and 665 nm, respectively, since this Index provides information about the amount of vegetation,

Table 1. Summary of tasks.

Objective	Tasks
1. Measuring total forest and deforested areas	T1.1: Downloading 4 SAR products from Sentinel-1B. T1.2: Pre-processing SAR products with Graph Builder in SNAP. T1.3: Supervised Classification of SAR products with Random Forest. T1.4: Post-Processing of Labelled Classes to remove random noise using a Morphological Filter “Closing 3x3”. T1.5: Exporting clean RF product to GeoTIFF for visualization with QGIS. T1.6: Creation of a 2017–2020 Time Series of Deforested areas in SNAP. T1.7: Calculation of Forested and Deforested areas of RF processed products with SNAP and “Raster Layer unique values report” with QGIS, comparing both results.
2. Measuring vegetation’s health, calculating the Vegetation Spectral Reflectance Curve	T2.1: Downloading 4 Multispectral products from Sentinel-2A. T2.2: Atmospheric correction of two “Level 1C” products obtained from Sentinel-2 using the “Sen2Cor” processor in SNAP. T2.3: Pre-processing of Multispectral products with Graph Builder in SNAP. T2.4: Measuring Vegetation’s Health by calculating Normalized Difference Vegetation Index (NDVI) in SNAP. T2.5: MSI Vegetation Analysis of RGB images and calculation of Colour Rough Statistic curves in SNAP for years 2017–2020. T2.6: Calculation of Spectral Reflectance Curve using the “Optical Spectrum View” in SNAP for 15 Regions of Interests (ROIs).
3. Calculating accuracy on measuring total forest and deforested areas	T3.1: Calculation of Confidence Value obtained with SAR products and Random Forest Classification in SNAP.

minimizing topographic effect and also distinguishing between soil and vegetation areas. It is based on the correlation among red and near-infrared (NIR) wavelengths since vigorous vegetation (green leaves) generally have a strong reflection in NIR and a strong absorption in RED bands.

A Synthetic Aperture Radar analysis and a Supervised Classification with a Random Forest algorithm using a Morphological Filter “Closing 3x3” for removing random noise were also undertaken over the same mining-affected area. Radar images were provided by Sentinel-1B satellite since it has an active C-band sensor (5.405 Ghz) on board. SNAP and QGIS v3.16 software were used for image visualization and management. Calculating total forest and deforested areas using the “Raster Layer unique values report” as well.

2.3.1. Study area

According to the information extracted from the Rainforest Action Network, there is a total of 32 oil sands companies in Canada [30]. In order to identify what company and projects could be more interesting for this study, a brief analysis of the literature was carried out, from which the following Table 2 was elaborated, including the names and volume of reserves of each oil sand producer.

Among these 20 companies, there are four companies that were blacklisted by the Norwegian sovereign wealth fund; Suncor Energy, Canadian Natural Resources (CNRL), Cenovus Energy and Imperial Oil. However, Suncor Energy is the company with the biggest volume of reserves, and therefore, it was chosen for this study to monitor the areas covered by its oil sands assets.

Table 2. Top-20 Oil Sand producers in Alberta–Canada. Reserves 2016 ([30] and own study).

Rank	Company	Reserves (barrels × 10 ⁶)	Rank	Company	Reserves (barrels × 10 ⁶)
1	Suncor Energy	10,935.35	11	Total	2575.16
2	Canadian Natural Resources (CNRL)	6867.53	12	Laricina Energy	2293.82
3	Cenovus Energy	5613.97	13	Sunshine Oilsands	2048.86
4	ConocoPhillips	5520.38	14	Imperial Oil	1694.29
5	ExxonMobil	4844.35	15	CNOOC	1655.91
6	Shell	3670.18	16	BP	1271.27
7	PetroChina	3225.71	17	Marathon Oil	1232.01
8	Athabasca Oil Corporation	3162.50	18	Devon Energy	1206.83
9	MEG Energy	2973.10	19	Husky Energy	1110.44
10	OSUM	2776.40	20	Chevron	1088.93

Table 3. Suncor Energy's oil sands assets in Alberta and status/type ([31] and own study).

#	Project Name	Status/Type	#	Project Name	Status/Type
1	MacKay River	In-situ	7	Syncrude Mine	Mining
2	Suncor Oil Sands (Dover)	In-situ	8	Voyageur South mining lease	Mining
3	Firebag	In-situ	9	Joslyn oil sands mining project	Mining
4	Fort Hills Oil Sands Project	Mining	10	Wapisiw Lookout	Reclamation
5	Millennium	Mining	11	Nikanotee Fen	Reclamation
6	North Steepbank	Mining	12	Base Mine Extension (Lewis)	Application process

Table 3 presents a summary of the oil sands assets either fully or partially owned by Suncor Energy Company. This table delineates each project's name and status/type. The first column is dedicated to enlisting the project names, while the second column provides information regarding the status or type of each project, which may vary depending on the project. The term "In-situ" indicates a technique of oil sands extraction wherein the bitumen is heated underground and subsequently extracted through wells. On the other hand, "Mining" indicates the use of traditional mining methods to extract oil sands. Lastly, "Reclamation" pertains to the process of restoring the land post-oil sands extraction. This process involves rehabilitating the affected areas by mining operations and the re-establishment of the ecosystems. "Application process" indicates that the project is in the application

stage, and the necessary permits to start the mining operations are not granted yet.

Figure 1 illustrates the location of oil sands and Suncor Energy's projects in Alberta.

2.3.2. Data used

Sentinel-1 and Sentinel-2 data used in this study were downloaded from the ESA SciHUB, <https://scihub.copernicus.eu/>, using different search parameters as shown in Table 4.

A total of 4 Sentinel-1B images and 4 Sentinel-2 images corresponding to a four-years period between 2017 and 2020 covering the area of interest were acquired and analyzed. Table 5 below contains all images used, including reference and date. Figure 2 shows the location map of the Sentinel-1 (red) and Sentinel-2 (green) images obtained from [21] and used for this study.

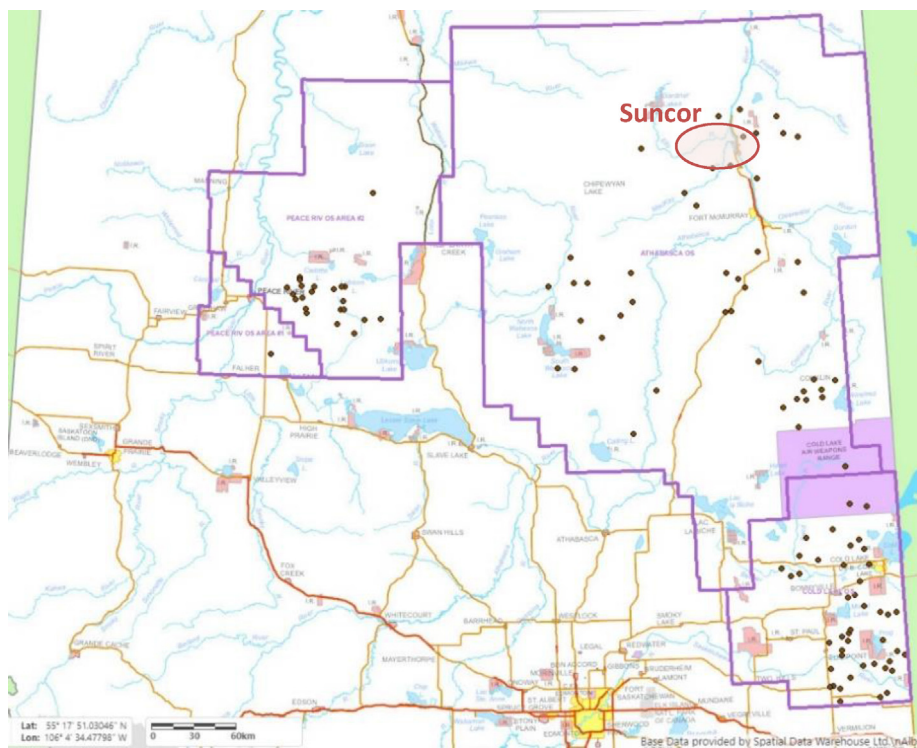


Fig. 1. Location of oil sands projects and Suncor Energy's oil sands assets in Alberta [32].

Table 4. Search parameters [33].

Sentinel-1	Sentinel-2
Sensing period: month of August from 2017 to 2020.	Sensing period: months of July and August from 2017 to 2020.
Check Mission: Sentinel-1	Check Mission: Sentinel-2
Product Type: GRD	Cloud Cover %: [0 TO 10]
Sensor Mode: IW	

Since the area of interest is affected by unfavourable weather conditions and mostly covered by snow during the winter season, this study gave priority to satellite images obtained during the summer season, particularly during the months of July and August. So that results obtained from

Sentinel-1 could be compared with the Sentinel-2 images acquired more or less during the same time period. Therefore, at least one image per year per each sentinel satellite was collected for a total period of four years, from 2017 to 2020.

Sentinel-1 satellites are formed by a constellation of two polar-orbiting satellites (1A and 1B), which are phased at 180° to each other. They have an active sensor (radar) that works on the seabed and provides data with a short repeat cycle with different imaging modes. The maximum time gap a user can have is five to 6 day at the Ecuador level. Sentinel-1 is an all-weather satellite capable of capturing whole-day radar images, either for land and ocean uses. Sentinel-1A was launched on April 3, 2014 and

Table 5. Sentinel data used in this study [33].

Satellite	Date	Image ID
Sentinel-1B	03/08/2020	S1B_IW_GRDH_1SDV_20200803T010645_20200803T010710_022752_02B2E3_0E08
Sentinel-1B	09/08/2019	S1B_IW_GRDH_1SDV_20190809T010639_20190809T010704_017502_020EAO_2660
Sentinel-1B	02/08/2018	S1B_IW_GRDH_1SDV_20180802T010632_20180802T010657_012077_0163CE_B268
Sentinel-1B	07/08/2017	S1B_IW_GRDH_1SDV_20170807T010626_20170807T010651_006827_00C043_6DF3
Sentinel-2A	19/08/2020	S2A_MSIL2A_20200819T183921_N0214_R070_T12VVJ_20200819T230508
Sentinel-2A	26/07/2019	S2A_MSIL2A_20190726T183921_N0213_R070_T12VVJ_20190726T230117
Sentinel-2A	11/07/2018	S2A_MSIL1C_20180711T183921_N0206_R070_T12VVJ_20180711T234527
Sentinel-2A	05/08/2017	S2A_MSIL1C_20170805T183921_N0205_R070_T12VVJ_20170805T183919



Fig. 2. Location map of the Sentinel-1 (red) and Sentinel-2 (green) images ([33] and own study).

Sentinel-1B two years later, on April 25. They were launched into orbit from the European Space port in French Guiana in a Soyuz rocket [34].

Sentinel-2 satellites are a group of two satellites, 2A and 2B, placed in a polar orbit with a 180° phase between each other. They have a Multispectral instrument capable of exploring 13 spectral bands (from 400 nm to 2200 nm wavelength) with a spatial resolution of 10, 20 and 60 m and a revisit time of 5 day at Ecuador. They are capable of providing multispectral high-resolution images useful for monitoring soil, water and vegetation cover as well as for being used in emergency situations. Sentinel-2A was taken into orbit on June 23rd, 2015, and Sentinel-2B on March 7th, 2017 [35].

2.3.3. Workflow

The workflow carried out in this study was split into two different parts, and all data processed was grouped into two categories of tasks. One main group (SAR Data) was required to pre-process SAR images from the Sentinel-1 satellite, and the second group (MULTISPECTRAL Data) was used for describing the pre-processing steps undertaken for the Sentinel-2 multispectral images.

2.3.3.1. SAR data. All acquired SAR images were opened in a SNAP session, which is a file that will open a list of specific products that were selected and predefined in advance. After opening the image “S1B_IW_GRDH_1SDV_20170807-T010626_20170807T010651_006827_00C043_6DF3”, in the “Product Explorer”, the SAR image was created for “Intensity VV”.

2.3.3.2. Pre-processing

2.3.3.2.1. Graph Builder. Once the image was created, the tool known as “Graph Builder” was used to carry out some pre-processing procedures on the acquired image prior to its analysis. The advantage of using the “Graph Builder” tool provided by SNAP is that some pre-processing steps can be automatized to use them with all images that will be processed in a later stage. Thus, a process of operators and algorithms needed to apply to the images was also specified. It has many advantages since a chain of operators can be defined so that they are entirely applied to the list of products previously selected. Another important advantage is that only the final product of this chain will be

created, saving storage capacity for the intermediate steps.

All the operators and the pre-processing chain created are shown in Figure 3 below.

2.3.3.2.2. Batch processing. By automating the execution of multiple processing steps on a set of data or files, the efficient and consistent application of various operations without manual intervention for each individual file is allowed. Table 6 shows a brief description of all operators included in the pre-processing chain of SAR images.

2.3.3.2.3. Random Forest classification. Once all SAR images were pre-processed (see Figure 4) using the chain described before, a Supervised Classification process using for this purpose SNAP software and a machine learning algorithm called “Random Forest” (RF) was undertaken. RF is commonly used as a machine learning technique for classification. It helps to separate forest and non-forest areas for each product obtained from Sentinel-1B, shown in Table 5. Thus, the classification process started by opening an RGB image Window to better identify the areas of interest, in which different rectangles linked to three new “Vector Data Containers” named “Oil”, “Deforested”, and “Forested” were drawn and saved as “Shape” files. They will be the training data used to train the machine learning model so that it can learn the relation between the input data and the final one.

The classification process started by picking the first Sentinel-1B product that was previously pre-processed in the SNAP’s window “product explorer”. The first product was the product “Subset_S1B_IW_GRDH_1SDV_20170807T010626_20170807T010651_006827_00C043_6DF3_Orb_NR_Cal_Sp_k_TC_Sigma0_VH”. Then, by clicking in the menu option “Vector/Import/ESRI Shapefile” and navigating to the folder “AuxData”, shape files “Oil.shp”, “Deforested.shp” and “Forested.shp” were selected. In the SNAP’s window “Import Geometry”, option “No” was selected and product was saved. Since the purpose of this research is to analyze the evolution of deforestation, an independent classification was run for every product. Thus, the same procedure described before was repeated for all pre-processed products from Sentinel-1B. Source products are shown in Figure 5 below.

The next step was to start the Random Forest Classifier in the SNAP’s top menu Raster/Classification/Supervised Classification/Random Forest Classifier. “Random Forest” (RF) machine learning



Fig. 3. Operators’ chain used during the pre-processing of SAR images.

Table 6. Operators used in the pre-processing chain.

Operator	Description
Apply Orbit File	Used to update orbit state vectors of the acquired product since orbit state vectors provided in the metadata of a product are generally not accurate and can be refined. Thus, it provides accurate information on satellite position and velocity, therefore improving the analysis. Option “do not fail if new orbit file is not found” was selected.
Thermal Noise Removal	The background energy that usually is generated by its own receiver is called “Thermal noise”. This aspect is important to be taken into account since it makes the radar reflectivity to move higher values. Also, it could be an obstacle that could affect the precision of any estimate made on radar reflectivity. So basically, in this step, part of the inner noise that appears in the data will be removed.
Calibration	This step is a basic step since, thanks to calibration process, calibrated SAR images with radiometric corrections can be obtained. Therefore, pixel values can be directly related to the radar backscatter of the scene. This is essential for quantitative use or comparison of SAR data that, for instance, may be obtained using different sensors.
Speckle Filtering	Sometimes, speckle filtering is unnecessary since it depends on the application and aim of the images. It is attributed to random interferences of the coherent return waves. Basically, there are two types: multilook processing or spatial filtering. For this study, the default speckle filter provided by SNAP was used.
Terrain Correction	All distances in SAR images are in radar geometry still. They can be distorted and should be corrected to compensate for any topographical variation or distortions. Also, it is important to define the cartographic system and preferred map projection. Map projection UTM/WGS 84 was selected.
Subset	The subset operator was selected to reduce the size and extension of the final product. Coordinates used: POLYGON ((-112.09469604492188 56.81134033203125, -110.77399444580078 56.81134033203125, -110.77399444580078 57.49019241333008, -112.09469604492188 57.49019241333008, -112.09469604492188 56.81134033203125, -112.09469604492188 56.81134033203125))
Write	This operator was used to write and save the final product.

algorithm is effective either for regression or classification by trying to learn the existing relationship between training and resulting dataset.

In the Random Forest Classifier window, the first pre-processed image “Subset_S1B_IW_GRDH_1SDV_20170807T010626_20170807T010651_006827_00C043_6DF3_Orb_NR_Cal_Spk_TC” was added to the ProductSet-Reader tab. In the Random Forest Classifier tab, the options selected are shown in [Table 7](#) below.

In the “Write” tab, the “Processed Products” directory was selected as the output folder, using the “2017_RF_LabelledClasses” name for the output file before clicking on the “Run” button. This process was repeated for the other three pre-processed products from years 2018, 2019 and 2020, respectively.

After creating the RF products, in the SNAP’s window, the “Product Explorer” and “Bands” folder were displayed to adjust the “properties”. By doing a right click on the “LabelledClasses” band and selecting the option “properties”. In the popup window, for the “Valid-Pixel Expression” option, the default value “Confidence \geq 0.5” was deleted. Also

the “No-Data Value Used” option was unselected and the product saved.

By doing double click on the “LabelledClasses” band, the result can be visualized. The original colour was adjusted by clicking the “colour manipulation” tab on the left-down window. Then, the “blue” colour was selected for the category “Deforested” of the year 2017. Reaching this point, the same process was repeated for the remaining images from years 2018, 2019 and 2020, while colours “green”, “orange”, and “red” were respectively selected for each year. After the process was finished, all pre-processed images from Sentinel-1B were closed, keeping only the classified products in the “Product Explorer” SNAP’s window. The results of this colour manipulation are depicted in [Section 3. “Results”](#).

2.3.3.3. Post-processing. As it can be seen in the image below [Figure 6](#), there is still some random noise. This inherent speckle noise that appears in the original data obtained with the SAR sensor and mistakenly classified as “Deforested” should be

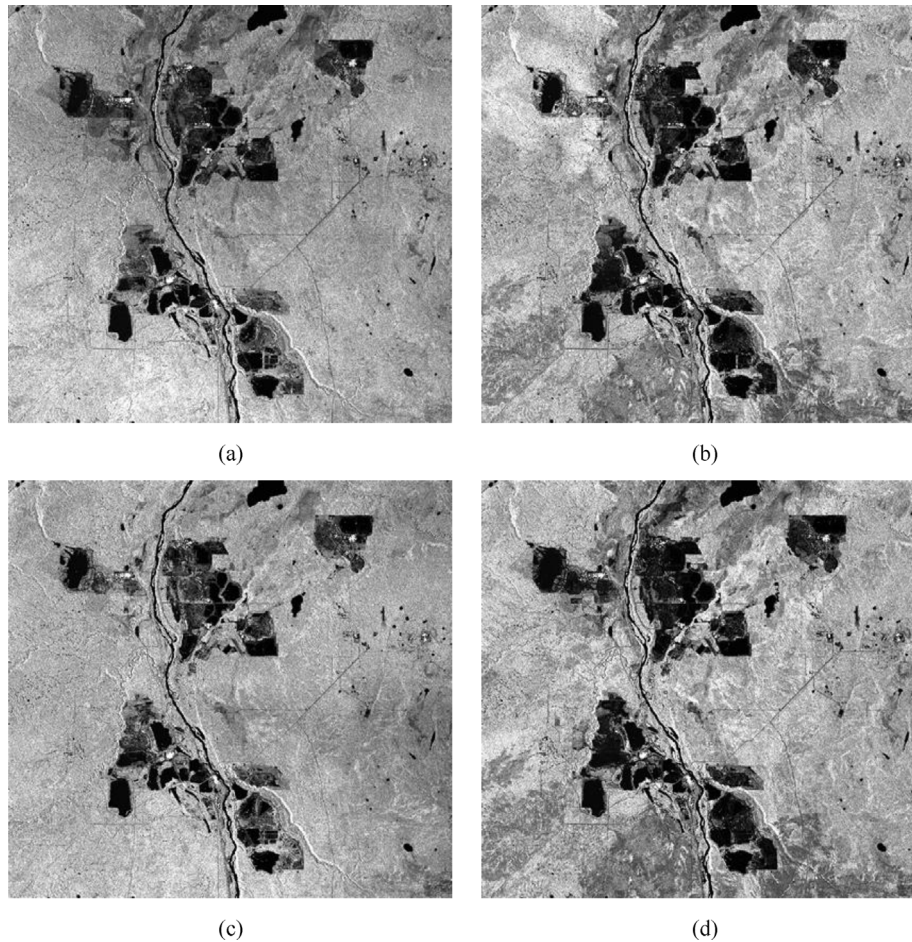


Fig. 4. Pre-processed products: (a) *Subset_S1B_IW_GRDH_1SDV_20170807T010626_20170807T010651_006827_00C043_6DF3_Orb_NR_Cal_Spk_TC_Sigma0_VH*; (b) *Subset_S1B_IW_GRDH_1SDV_20180802T010632_20180802T010657_012077_0163CE_B268_Orb_NR_Cal_Spk_TC_Sigma0_VH*; (c) *Subset_S1B_IW_GRDH_1SDV_20190809T010639_20190809T010704_017502_020EA0_2660_Orb_NR_Cal_Spk_TC_Sigma0_VH*; (d) *Subset_S1B_IW_GRDH_1SDV_20200803T010645_20200803T010710_022752_02B2E3_0E08_Orb_NR_Cal_Spk_TC_Sigma0_VH*.

removed in order to work with a cleaned dataset. For doing so, the closing “Dilation + Erosion” filter was used by expanding the first classified product “Subset_2017_RF” in the Product Explorer SNAP’s window. After that, the Bands folder was opened and clicked on the “LabelledClasses” band. In the Raster top menu, Filtered band menu was clicked, and then, the “Closing 3x3” option in the Morphological Filter that appears in the “System” tab was selected. Finally, the default name for the option “Band name” was also kept.

Now, in the Product Explorer window appears, the “LabelledClasses close3” under the Bands folder previously created. Then, on the top menu, the option “Windows/Tile Horizontally” was selected in order to visualize “LabelledClasses” and “LabelledClasses close3” simultaneously.

To export the product to GeoTIFF format, the first product “Subset_S1B_IW_GRDH_1SDV_20170807

T010626_20170807T010651_006827_00C043_6DF3_Orb_NR_Cal_Spk_TC_RF” of the Product Explorer SNAP’s window was selected before clicking on the “Export” and “GeoTIFF” submenus that appear in the “File” top menu. Once the “SNAP-Export Product” window was opened and clicked on the “Subnet” button on the “Band Subnet” tab, the option “LabelledClasses close3” was the only option selected before clicking on the “OK” and the “Export Product” buttons. A product related to the year 2017 was exported and named “RF_2017GEO”. This full process used for removing the random noise was repeated for the remaining products, which were also exported and renamed to “RF_2018GEO”, “RF_2019GEO”, and “RF_2020GEO”, respectively.

2.3.3.4. QGIS visualization. To visualize the evolution as time series 2017–2020 of deforested and non-deforested areas (see [Figures. 8 and 9](#)), QGIS 3.16

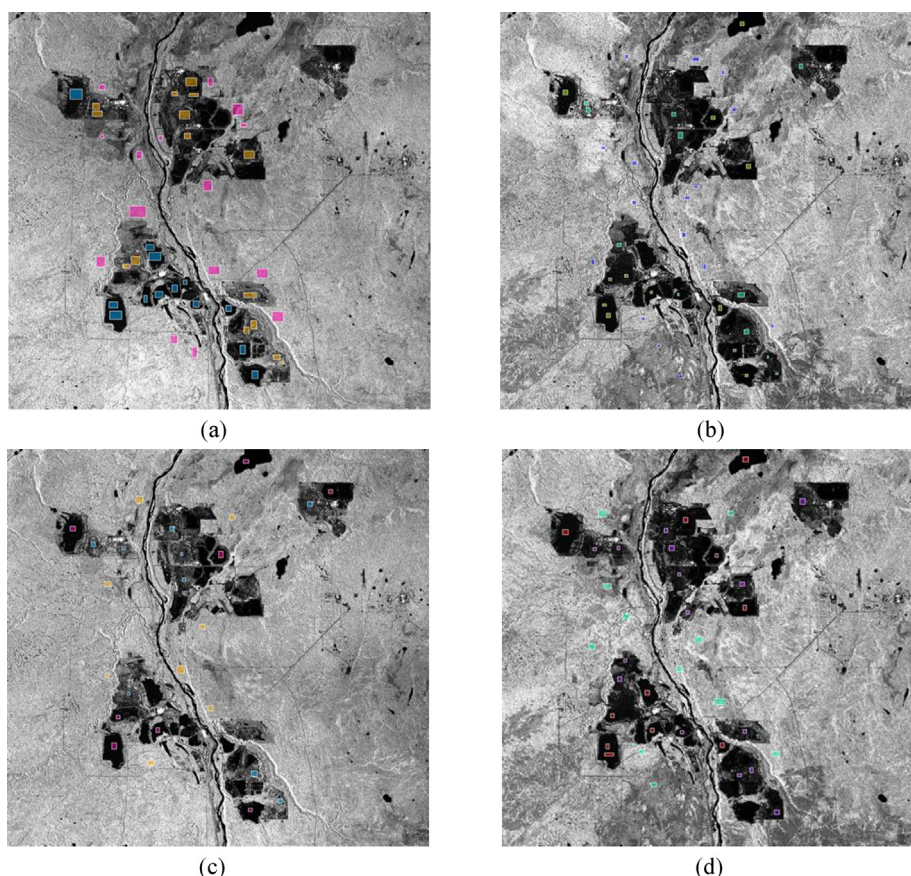


Fig. 5. Vector Data Containers of Images used for training data: (a) *Subset_S1B_IW_GRDH_1SDV_20170807T010626_20170807T010651_006827_00C043_6DF3_Orb_NR_Cal_Spk_TC_POL*; (b) *Subset_S1B_IW_GRDH_1SDV_20180802T010632_20180802T010657_012077_0163CE_B268_Orb_NR_Cal_Spk_TC_POL*; (c) *Subset_S1B_IW_GRDH_1SDV_20190809T010639_20190809T010704_017502_020EAO_2660_Orb_NR_Cal_Spk_TC_POL*; (d) *Subset_S1B_IW_GRDH_1SDV_20200803T010645_20200803T010710_022752_02B2E3_0E08_Orb_NR_Cal_Spk_TC_POL*.

software was used. The visualization process started by adding chronologically the Raster Layers related to each RF product in the “Layers Panel”. By placing the most recent product in the lower part of the “Layers Panel”.

Since each classified product is by default opened as a single band grey raster file, default “visualization” and “properties” of the following products

“RF_2017GEO”, “RF_2018GEO”, “RF_2019GEO”, and “RF_2020GEO” were adjusted according to the criteria shown in Table 8.

By pressing the “Classify” button and clicking on the “Load Color Map” icon, one own colour scheme was picked, selecting the “Color_QGIS_2017.txt” file and clicking the “OK” button. For the remaining “RF” products, the same procedure was followed, saving their color palettes as “Color_QGIS_2018.txt”, “Color_QGIS_2019.txt”, and “Color_QGIS_2020.txt” respectively.

2.3.3.4.1. *MULTISPECTRAL data.* The process started by launching SNAP software and opening the four zipped downloaded Sentinel-2A products described in Table 5 under section 2.3.2.

Once four products were opened in the “Product Explorer”, a file related to 2020 was selected by right-clicking on it and also on the option “Open RGB Image window”. A new window was opened in which the value “Sentinel 2 MSI Natural Colors” was selected in the “Profile” drop-down menu. After

Table 7. Options for the random forest classifier.

Option	Value
Train and apply classifier	Selected
Train on Vectors	Selected
Evaluate classifier	Un-checked
Evaluate Feature Power Set	Un-checked
Number of training samples	5000
Number of trees	500
Training vectors	All shapefiles selected
Feature bands	All bands selected

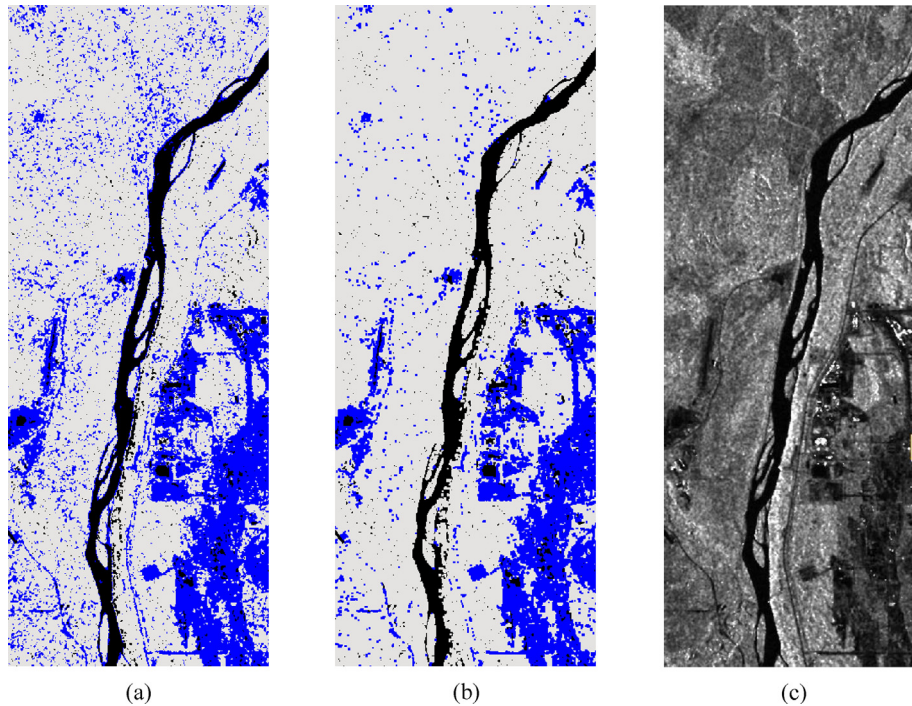


Fig. 6. Speckle Noise comparison using Closing 3x3 Morphological Filter: (a) 2017_RF_LabelledClasses; (b) 2017_RF_close3; (c) Subset_S1B_IW_GRDH_1SDV_20170807T010626_20170807T010651_006827_00C043_6DF3_Orb_NR_Cal_Spk_TC_POL.

this step, an RGB image was opened in the View section.

2.3.3.5. *Atmospheric correction.* Since two products related to the years 2017 and 2018 downloaded from the ESA SciHUB were “Level 1C” data, it was necessary to convert them to L2A products. Thus, they were geometrically and radiometrically corrected, including also ortho-rectification and spatial-registration. However, only more recent products from 2019 to 2020 were available and downloaded as Level 2A, which include atmospheric correction as well.

Atmospheric correction is particularly needed in those cases where we need to analyze and compare multi-temporal images, as it happens in our study case, since the radiation reflected at the Earth’s surface is generally modified by its interaction at the atmosphere level. Thus, the goal of this correction is basically to obtain true surface values at the bottom of the atmosphere, based on the top of the atmosphere values.

The “Sen2Cor” processor was used to carry out the atmospheric correction (terrain and cirrus as optional) for the “Top of atmosphere (TOA)” L1C products. Thus, for all data obtained from Sentinel-2A from years 2017 and 2018 previously downloaded, “Bottom of Atmosphere (BOA)” corrected reflectance images were created by using the “Sen2Cor” processor, previously mentioned.

The process started by installing the “Sen2Cor” processor since it was not installed by default in the SNAP 8.0 version. Once installed, the “Optical/Thematic Land Processing/Sen2Cor Processor/Sen2Cor280” top menu was selected. In the new window, under the “I/O parameters” tab, the “.SAFE” folder was selected for the L1C product of 2017 and the “MTD_MSIL1C.xml” file.

In the second tab titled “Processing Parameters”, the “Display execution output” option was selected, and changed the resolution to “ALL” before clicking on the “Run” button on the same window. After the image was processed, the process was repeated with



Fig. 7. Operators’ chain used during the pre-processing of multispectral images.

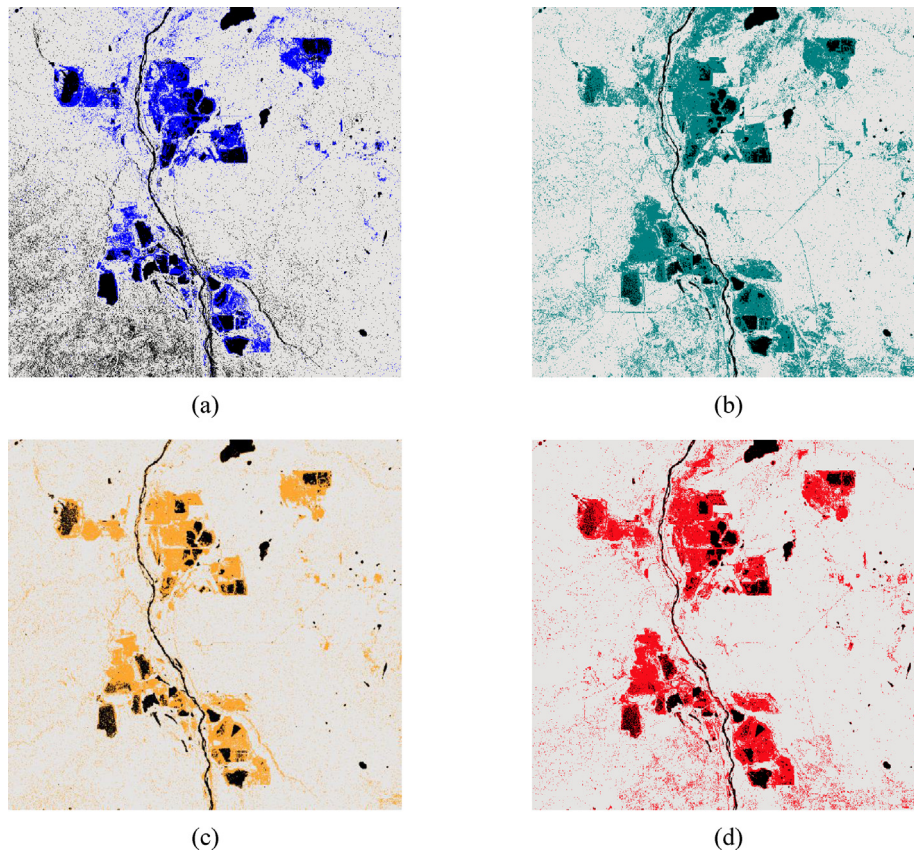


Fig. 8. RF Classified products without using Closing 3x3 Morphological Filter: (a) 2017_RF_LabeledClasses; (b) 2018_RF_LabeledClasses; (c) 2019_RF_LabeledClasses; (d) 2020_RF_LabeledClasses.

the other L1C product previously downloaded related to the year 2018. After finishing the process, two new products were created in the Product Explorer window, renamed as “Output Product 2017” and “Output Product 2018”, respectively. Then, these two new products were selected by right clicking on them, selecting the “Close 2 Products” option and clicking “No” in the next window to discard changes. The next step was to move the two new L2A products created in the.SAFE format in the original folder to the “Level 2A” folder. Results were loaded in the SNAP software by clicking on the.-SAFE format for years 2017 and 2018 only, and doing click in the “MTD_MSIL2A.xml” file for both years 2017 and 2018.

After having the four L2A products loaded in SNAP (year 2017, year 2018, year 2019 and year 2020) in the Product Explorer window, the L2A product from 2020 was opened as an RGB image. In the new window opened, the profile “Sentinel 2 MSI Natural Colors” was selected. To compare L1C products and L2A products together, the “Window/Tile Horizontally” top menu was clicked on as well. L1C products previously loaded in SNAP were closed since from now onward, only

L2A products will be required for the next processing steps.

2.3.3.6. Resample, subset & calculate. At this stage, the Graph Builder tool included in SNAP was used to speed up the process, avoiding going step by step. It was opened by clicking on the “Tools/Graph-Buildler” top menu.

Since the 13 working Bands of Sentinel-2 do not have the same resolution (size), and some operators of the GraphBuilder cannot work with products that have different sizes, it is necessary to resample all bands to have them first with the same resolution. Therefore, the operator “Resample” was added by right-clicking on the GrapBuilder and contextual menu “Add/Raster/Geometric/Resample”.

The “Subset” operator was also added to the GrapBuilder after the resampling by clicking on the contextual menu “Add/Raster/Geometric/Subset”. The other two operators, “BandMaths” and “Band-Merge”, were added and connected to the Graph-Buildler as shown in [Figure 7](#).

After all operators were added and connected to each other, the Graph was saved as an XML file in the “Processing” folder.

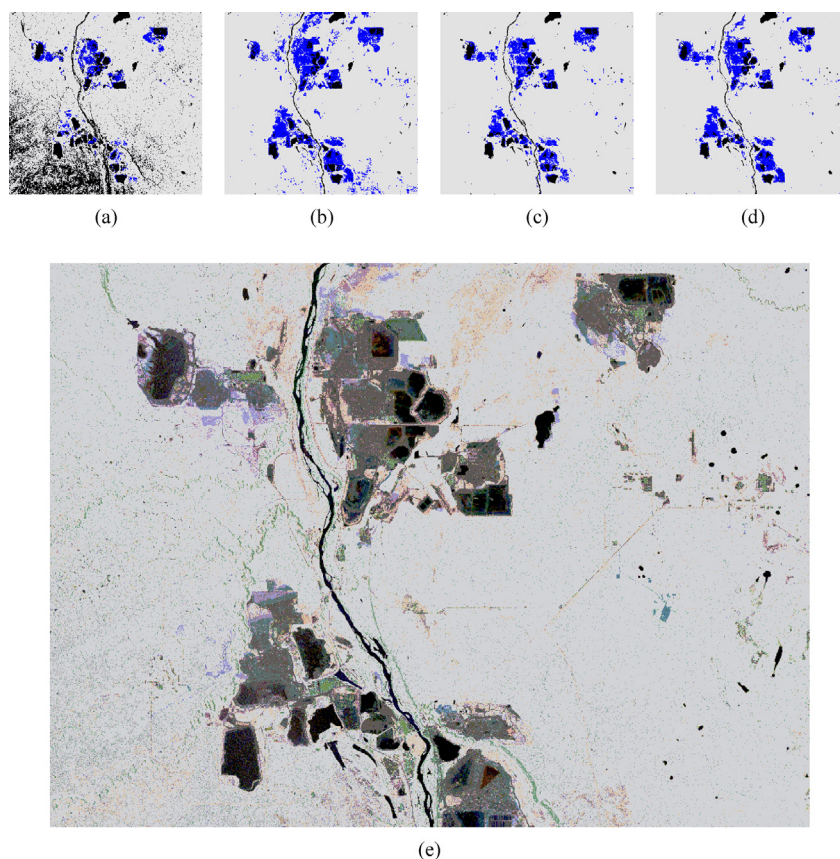


Fig. 9. GEOTIFF Images – after using Closing 3x3 Morphological Filter and 2017–2020 Time Series: (a) RF_2017GEO; (b) RF_2018GEO; (c) RF_2019GEO; (d) RF_2020GEO (e) RF_2017–2020 Time Series.

The processing parameters of each operator were the following.

The process was run and repeated for all four L2A products uploaded to SNAP, starting with the year 2020 and finishing with the year 2017. After expanding all products in the Product Explorer in SNAP, NDVI bands for each product were displayed, picked the colour ramp “Derived from JET” in the “Colour Manipulation” tab in SNAP, and then clicked on the “Window/Tile Horizontally” top menu and zoomed them all to compare all images better, see Figure 12 included in Section 3 “Results”. The same histogram stretch was used for all images by selecting the first view related to the year 2017 and

opening the “Colour Manipulation” tab in the lower left corner. The same process was followed for other bands and to NDVIs from years 2018, 2019 and 2020, too. After all these steps, images were ready to start the classification with QGIS software.

2.3.3.7. Measuring vegetation’s health. The Normalized Difference Vegetation Index (NDVI) is usually used to check the health and vitality of vegetation. It was developed by Rouse, J. W [36]. in 1974 and tells us information about the amount of vegetation, minimizing topographic effect and also distinguishing between soil and vegetation areas.

It is based on the correlation among red and near-infrared (NIR) wavelengths since vigorous vegetation (green leaves) generally have a strong reflection in NIR and a strong absorption in RED bands. For adding this NDVI band to the original subset, the “BandMerge” operator was used with the default values and the equation mentioned in Table 9.

Usually, NDVI runs from the scale of -1.0 to 1.0 , having the most vigorous vegetation within a range value of 0.66 – 1.0 . NDVI values close to 0.3 indicate the presence of shrubs and grassland, while NDVI values close to 0.0 correspond to sand, barren areas

Table 8. Options for the Layer Properties of each product.

Option	Value
Render Type	Singleband pseudocolor
Band	Band 1 Gy
Min value	0
Max value	1
Interpolation	Linear
Color	RdY/Gn
Mode	Equal interval
Classes	2

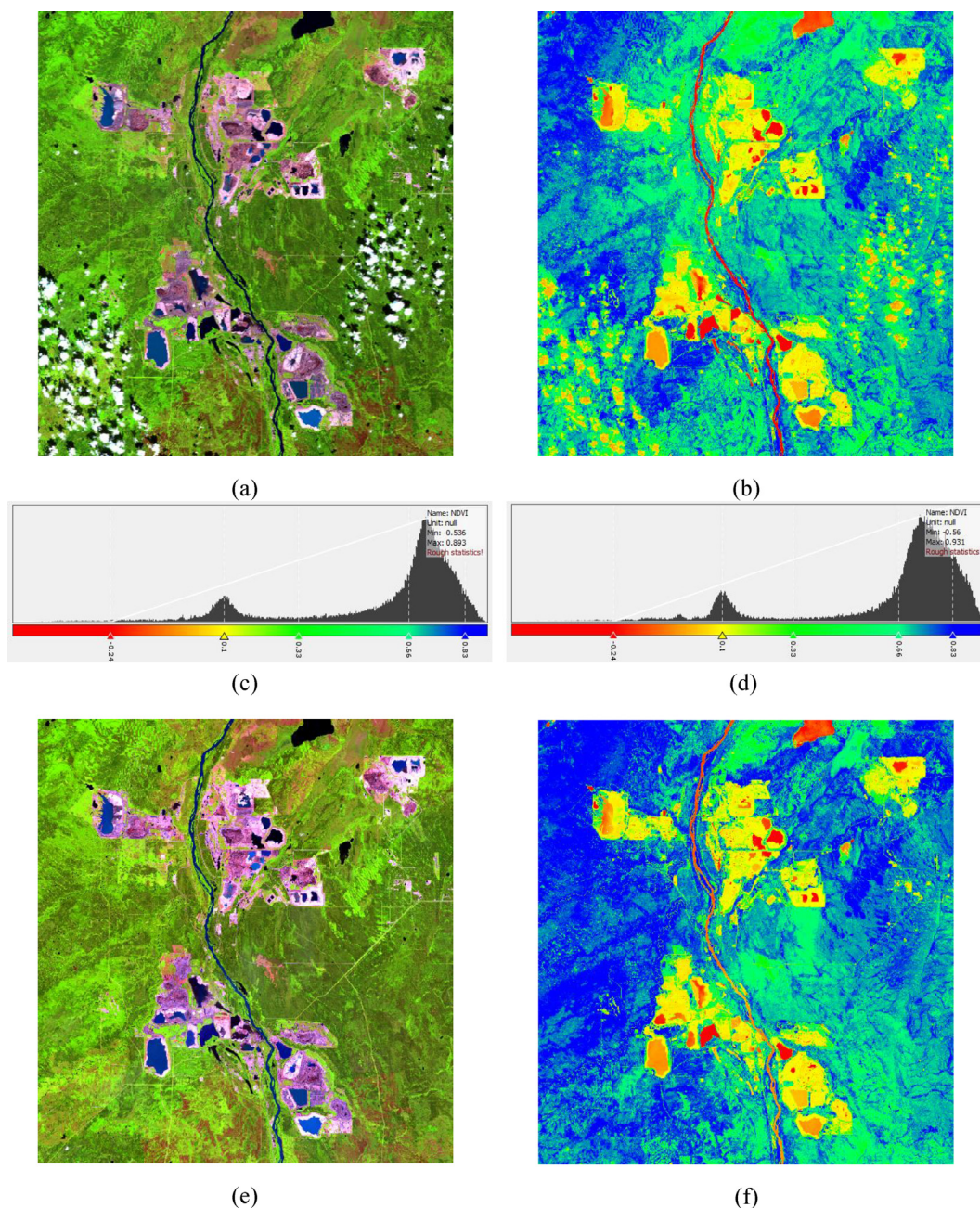


Fig. 10. MSI Vegetation Analysis RGB images, NDVI spectral index and Colour Rough Statistic curves for 2017 and 2018: (a) 2017_Resampled_RGB (Bands B11, B8, and B4); (b) 2017_NDVI; (c) 2017 NDVI Colour Rough Statistic Curve; (d) 2018 NDVI Colour Rough Statistic Curve; (e) 2018_Resampled_RGB (Bands B11, B8, and B4); (f) 2018_NDVI.

of rock, or snow. Finally, NDVI values close to -1.0 are related to water areas.

2.3.3.8. Calculation of NDVI index. After resampling, subset and calculation processes, a new layer called NDVI was added to each GEOTIFF product obtained for the years 2017–2020, together with the other bands B4, B8, B11 and B12. NDVI Index was calculated using the operator “BandMaths” in the

operator’s chain of the Graph Builder tool in SNAP. Parameters used for the BandMaths operator were described in Table 9.

The process started with the file from 2017 opening the NDVI band in SNAP. The colormap was edited using for this purpose the “Color Manipulation” tool included in the lower left corner. A colour band to NDVI values equal to 0.1, 0.33 and 0.66, respectively, was added and applied the same

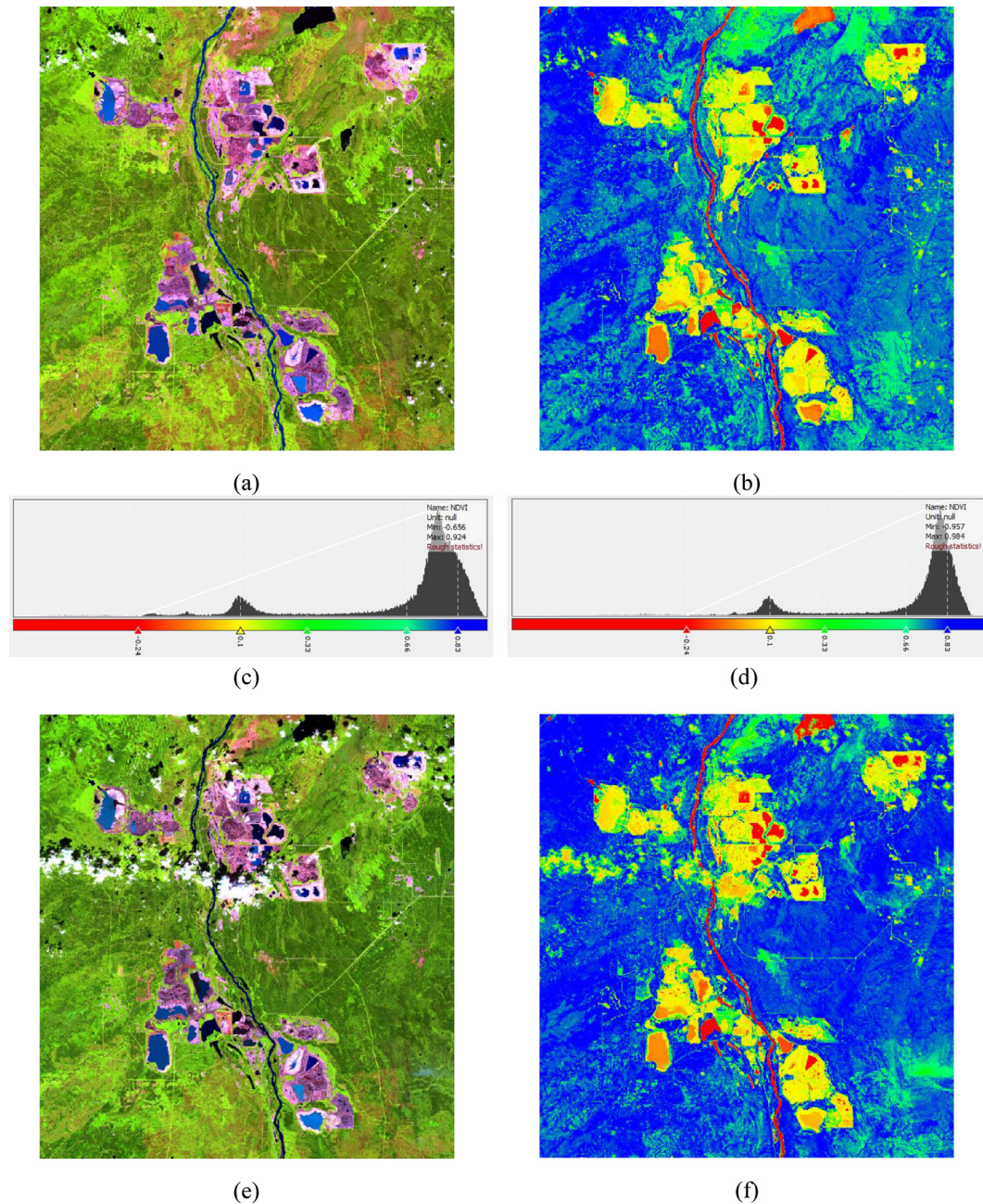


Fig. 11. MSI Vegetation Analysis RGB images, NDVI spectral index and Colour Rough Statistic curves for 2019 and 2020: (a) 2019_Resampled_RGB (Bands B11, B8, and B4); (b) 2019_NDVI; (c) 2019 NDVI Colour Rough Statistic Curve; (d) 2020 NDVI Colour Rough Statistic Curve; (e) 2020_Resampled_RGB (Bands B11, B8, and B4); (f) 2020_NDVI.

histogram stretch to NDVI calculated for years 2018, 2019 and 2020. The colour ramp “Derived from JET” was assigned to all NDVI products, and the results of this process are depicted in Figure 10, Figure 11, Table 13 and Section 3.

2.3.3.9. Calculation of spectral curves of ROIs. For calculating the Spectral curves of the 15 regions of interest (ROI) in the surrounding area of the Suncor

mining permits, a total of 15 ROIs were randomly picked over the L2A product related to the year 2020 previously downloaded from Sentinel-2A “S2A_MSIL2A_20200819T183921_N0214_R070_T12VVJ_20200819T230508”.

L2A product containing spectral information was opened in SNAP 8.0 in order to use the twelve spectral bands included in the product data. The shortlist of 15 ROIs and their Geographic

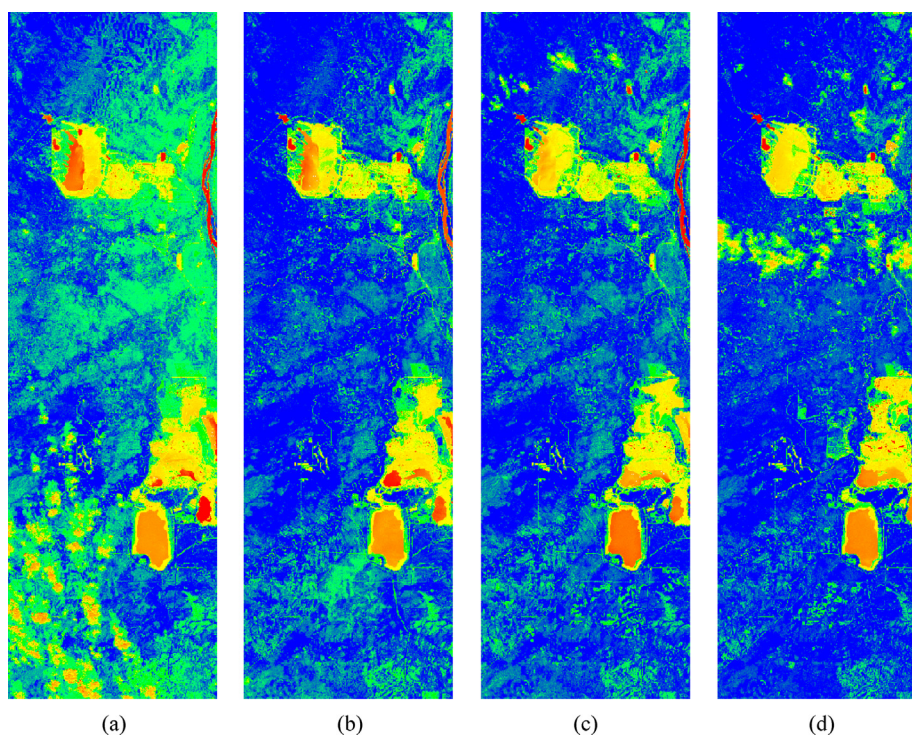


Fig. 12. NDVI detail images for years 2017, 2018, 2019 and 2020 after using the same histogram stretch (colour manipulation): (a) 2017_NDVI; (b) 2018_NDVI; (c) 2019_NDVI; (d) 2020_NDVI.

Coordinates are shown in Figure 13. Spectral Reflectance Curve was automatically calculated using the “Pins” and “Optical Spectrum View” tools in SNAP 8.0 for the 15 Regions of Interests (ROIs) shown in Figure 14 in Section 3 “Results”.

For placing the 15 pins over the L2A product image, the “Pin Manager” tool was opened by clicking on the upper horizontal menu “View/Tool Windows/Pin Manager” in SNAP. Pixel position (X, Y) and also geographical coordinates of each pin were displayed in the pin manager and shown in Figure 13. Colour of each pin linked to specific ROIs was colored and renamed according to the study’s needs and the researcher’s criteria.

3. Results

3.1. SAR analysis

Table 10 below shows frequency values and level of confidence obtained for each classified product after executing the RF classification process in SNAP.

The result of changing the colour of the RF classified products is shown in Figure 8 below.

For calculating deforested areas for each class from years 2017–2020, the tool and algorithm “Raster layer unique values report” was utilized,

which is included as default in the software QGIS. Values obtained are shown in Table 11 below.

By comparison of the results obtained with the program SNAP and the data obtained in QGIS after using the algorithm “Raster layer unique values report”, it is observed a small difference each year, due mainly to the speckle noise removed with the Closing 3x3 Morphological Filter. Table 12 shows the differences between both values expressed in percentage of variation.

As can be seen in the table, the average variation between QGIS and SNAP values varies in the range of -2.42% and $+2.37\%$, both values obtained for the year 2019.

4. Discussion

After performing the analysis of the SAR and Multispectral data obtained from sentinel-1B and sentinel-2A satellites, the discussion focuses on the SAR data obtained from S-1B for the year 2017. According to this, it was found interesting the result of GEOTIFF images obtained after using the Closing3x3 Morphological Filter and being exported to QGIS shown in Figure 9. As can be seen, the 2017–2020 Time Series shows different colored areas representing deforested areas for each year from 2017 to 2020. The black colour was used to

Table 9. Options used for the operators in the Graph Builder for each product.

Operator/Options	Value
RESAMPLE TAB	
Define size of resampled product	B11 (all bands to 20 m resolution)
By reference band from source product	Checked
Downsampling method	Mean
Resample on pyramid levels	Checked
SUBSET TAB	
Bands B4, B8, B11 and B12	Selected
Copy metadata	Checked
Geographic coordinates	Checked
Coordinates	Subset operator was selected to reduce the size and extension of the final product. Coordinates used: POLYGON ((-112.09469604492188 56.81134033203125, -110.93000000 56.81134033203125, -110.93000000 57.49019241333008, -112.09469604492188 57.49019241333008, -112.09469604492188 56.81134033203125, -112.09469604492188 56.81134033203125))
BANDMATH TAB	
Target band	Normalized Difference Vegetation Index (NDVI)
No-data value	0.0
Edit Expression	$(B8 - B4)/(B8 + B4)$ This formula was obtained from $NDVI = (NIR - Red)/(NIR + Red)$
Show bands	Checked
BANDMERGE TAB	
All settings	Used the default value (no change)
WRITE TAB	
Save as	GeoTIFF
Output directory	... /Processed products

indicate those areas flooded either by oil and/or water.

In the image [Figure 9a](#), related to the year 2017, there was a massive area in the lower left corner apparently flooded by water or oil. It indicates this area was likely covered by vegetation and perhaps water simultaneously since, according to the data shown in [Tables 11 and 12](#), the obtained value in 2017 for the water/oil-covered area, i.e. 10.60% and 11.49% (SNAP and QGIS), was significantly higher than values obtained for years 2018, 2019 and 2020 (3.05%, 3.30% and 3.15% respectively). It was

probably because, during the year 2017, the groundwater table was higher than in other years, or perhaps because there was a terrestrial oil spill that covered such area, or a dense vegetation that reduced radar backscatter, appearing as dark spots on the image.

In order to find out the origin of such dark spots, whether they were caused by water, oil or dense vegetation, the Normalized difference water index (NDWI) [37] was calculated using for this purpose Sentinel-2 MSI images and QGIS software.

[Figure 15](#) shows the 12 spectral bands of the Sentinel-2 MSI instrument. Band 8 in the near-infrared and band 3 in the visible band will be used to calculate the NDWI.

To understand why these wavelengths are used to identify water, it makes sense to look at the reflectance Spectra of water that is shown in [Figure 16](#) below.

The black lines show wavelength on the x-axis and reflectance on the y-axis. The lowermost black line is for relatively pure water with low total dissolved solids or low turbidity at 35 mg per litre. This pure water has a relatively high reflectance in the green and low reflectance in the infrared.

Once the L1C (ToA) product related to the year 2017 was downloaded from Sentinel-2A, it was geometrically and radiometrically corrected, including also ortho-rectification and spatial registration using the “Sen2Cor” processor to obtain a L2A (BoA) product, as it is shown in [Figure 17a](#).

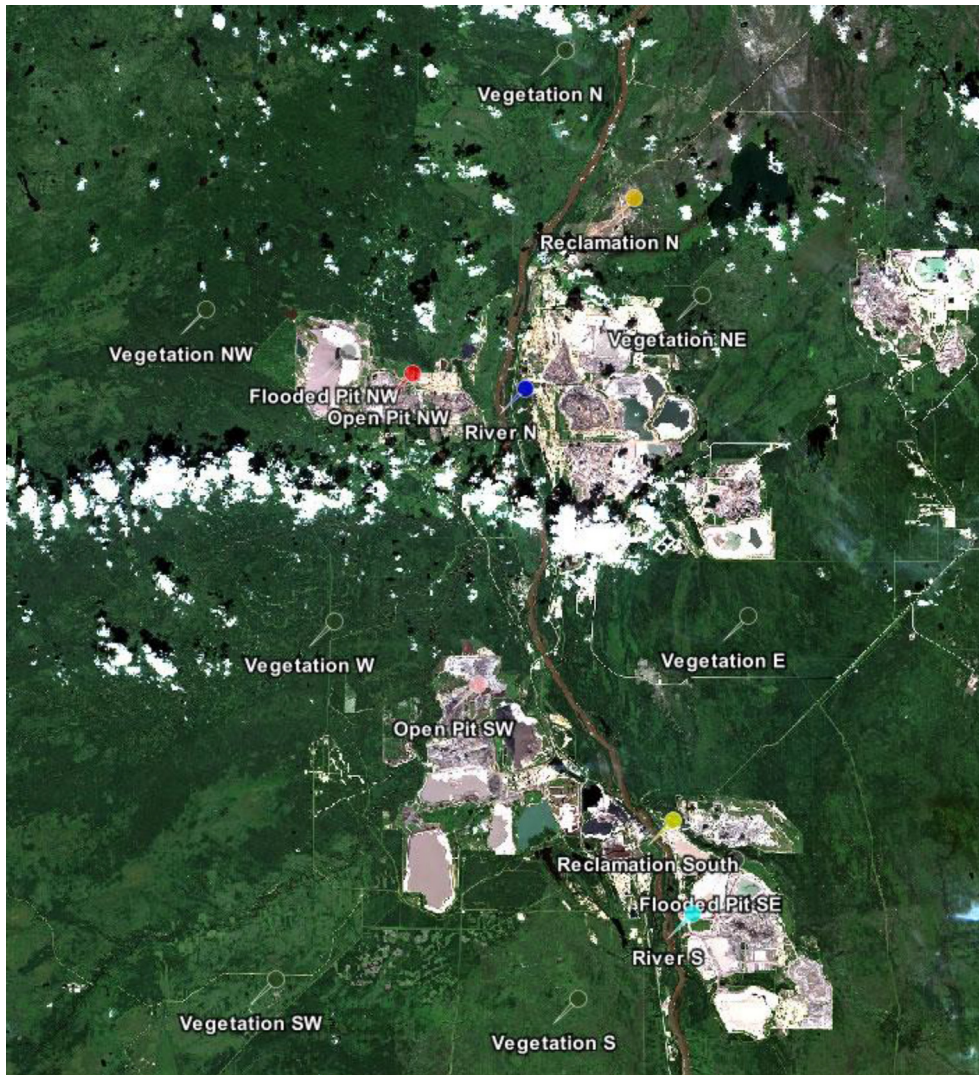
The NDWI was calculated using the formula below [37] in the QGIS raster calculator.

$$NDWI = \frac{[Green - NIR]}{[Green + NIR]} = \frac{[B3 - B8]}{[B3 + B8]}$$

The result of applying this formula is depicted in [Figure 17b](#). After adjusting raster symbology to identify an NDWI threshold that discriminates water pixels, the raster calculator was used to assign high NDWI pixels the value of 1, and all other pixels a value of 0.

By doing a right-click over the layer properties in QGIS, the symbology tab was opened. The “Render type” option was set as “singleband pseudocolor”, and the “Interpolation” to “Discrete” to be able to establish thresholds below which or above which the pixels have a certain color. Two discrete intervals were created, selecting 1.5 for the upper end and 0.07 to the low end. Thus, anything below or equal to 0.07 is cleared, and anything above 0.07 is colored in blue to show it as water.

Water bodies and flooded areas were properly identified in [Figure 17b](#). Results of the visual



(a)

X	Y	Lon	Lat	Color	Label
4364.500	6675.500	-111.931844	57.139187		Vegetation W
3879.500	9644.500	-112.004754	56.871888		Vegetation SW
6389.500	9806.500	-111.592780	56.859968		Vegetation S
3300.500	4098.500	-112.114586	57.369210		Vegetation NW
7414.500	3976.500	-111.430722	57.384366		Vegetation NE
6278.500	1942.500	-111.622767	57.566277		Vegetation N
7793.500	6637.500	-111.365309	57.145530		Vegetation E
7333.500	9102.500	-111.438710	56.923850		River S
5950.500	4746.500	-111.672953	57.314133		River N
7172.500	8327.500	-111.466026	56.993375		Reclamation South
6852.500	3171.500	-111.525232	57.456320		Reclamation N
5558.500	7204.500	-111.733634	57.092980		Open Pit SW
5016.500	4624.500	-111.828243	57.324166		Open Pit NW
7685.500	8658.500	-111.381292	56.963926		Flooded Pit SE
4483.500	4446.500	-111.917141	57.339540		Flooded Pit NW

(b)

Fig. 13. Regions of interest (ROIs) map and description table with geographic coordinates: (a) S2A_MSIL2A_20200819T183921_N0214_R070_T12VVJ_20200819T230508; (b) ROF's coordinates.

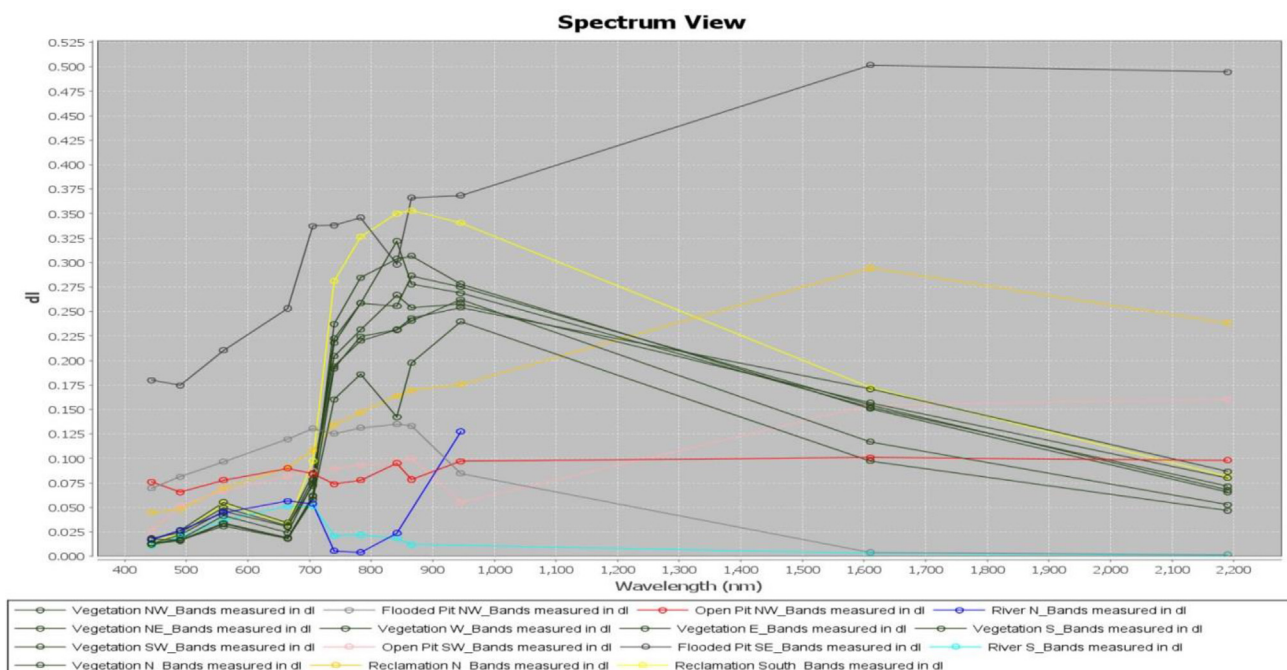


Fig. 14. Spectral curve of ROIs.

Table 10. Frequency values and level of confidence per category and year obtained using SNAP.

Category	2017	2018	2019	2020				
No Data	0%	Conf.	0%	Conf.	0%	Conf.	0%	Conf.
Deforested	7.75%	55.58%	19.86%	52.34%	13.63%	52.73%	13.30%	52.93%
Forested	81.65%	77.79%	77.09%	76.17%	83.07%	76.37%	83.55%	76.46%
Water/Oil	10.60%	100%	3.05%	100%	3.30%	100%	3.15%	100%
Total	100%		100%		100%		100%	

analysis of the blue-colored areas indicate that there is a mismatch between the dark spots that appeared in the bottom left corner of Figure 9a obtained after processing the Sentinel-1B radar image from the year 2017 and the results obtained from the NDWI analysis to identify water flooded areas. Therefore, a

further analysis is required to identify if the dark spot areas mentioned before were caused by terrain oil spills or if they should be considered false positives.

For this purpose, a total of three Prolife Plots (#1, #2, and #3) were placed over the radar image

Table 11. Raster layer unique values report obtained from QGIS.

	2017	2018	2019	2020
Projection	EPSG:32612 – WGS 84/ UTM zone 12N	EPSG:32612 – WGS 84/ UTM zone 12N	EPSG:32612 – WGS 84/ UTM zone 12N	EPSG:32612 – WGS 84/ UTM zone 12N
Width in pixels	8064 (units per pixel 10)	8064 (units per pixel 10)	8065 (units per pixel 10)	8064 (units per pixel 10)
Height in pixels	7608 (units per pixel 10)	7608 (units per pixel 10)	7608 (units per pixel 10)	7609 (units per pixel 10)
Total pixel count	61,350,912	61,350,912	61,358,520	61,358,976
Deforested: (Ha)/%	42,347.11 Ha 6.90%	110,169.8 Ha 17.96%	68,770.45 Ha 11.21%	73,837.43 Ha 12.03%
Forested: (Ha)/%	500,699.85 Ha 81.61%	484,410.87 Ha 78.96%	524,250.18 Ha 85.44%	520,284.16 Ha 84.79%
Oil/Water: (Ha)/%	70,462.16 Ha 11.49%	18,928.45 Ha 3.09%	20,564.57 Ha 3.35%	19,468.17 Ha 3.17%
Total	613,509 Ha 100%	613,509 Ha 100%	613,585 Ha 100%	613,590 Ha 100%

Table 12. Comparison of QGIS vs SNAP values.

CLASS	2017			2018		
	SNAP	QGIS	Var.	SNAP	QGIS	Var.
Deforested %	7.75	6.90	-0.85	19.86	17.96	-1.90
Forested %	81.65	81.61	-0.04	77.09	78.96	1.87
Oil/Water %	10.60	11.49	0.89	3.05	3.09	0.04
CLASS	2019			2020		
	SNAP	QGIS	Var.	SNAP	QGIS	Var.
Deforested %	13.63	11.21	-2.42	13.30	12.03	-1.27
Forested %	83.07	85.44	2.37	83.55	84.79	1.24
Oil/Water %	3.30	3.35	0.05	3.15	3.17	0.02

Table 13. NDVI – minimum and maximum values for years 2017–2020.

NDVI minimum and maximum values				
	2017	2018	2019	2020
NDVI min	-0.536	-0.560	-0.656	-0.957
NDVI max	0.893	0.931	0.924	0.984

S1B_IW_GRDH_1SDV_20170807T010626_20170807-T010651_006827_00C043_6DF3 previously processed and obtained from Sentinel-1B. They were located in three different areas where the dark spots appeared

after using RF Classification and Closing 3x3 Morphological Filter (Figure 9a). The exact location of the three profile plots is depicted in Figure 18.

In order to analyze the Sigma0_VV intensity along the profile plots, the SNAP tool was used, resulting in three intensity backscatter graphs as depicted in Figure 19. Areas flooded by oil or water usually have close to zero Sigma0_VV values while highly dense vegetation areas present higher values of Sigma0_VV.

Figure 19b shows the path of the Profile Plot #2 from pixel 0 to pixel 2500. As can be seen, there is a section between pixel 1275 (point 1) and 1900 (point 2) in which Sigma0_VV values are very close to zero. This section corresponds to an area in which the backscattering reflectance of radar waves was reduced due to the presence of liquid, mostly oily materials since their reflectance values were slightly higher than clean water.

Two different sections appear in Figure 19c with almost zero Sigma0_VV values, indicating that these two areas of Profile Plot #3 are covered by a liquid element. Identifying these two areas in Figures. 17b

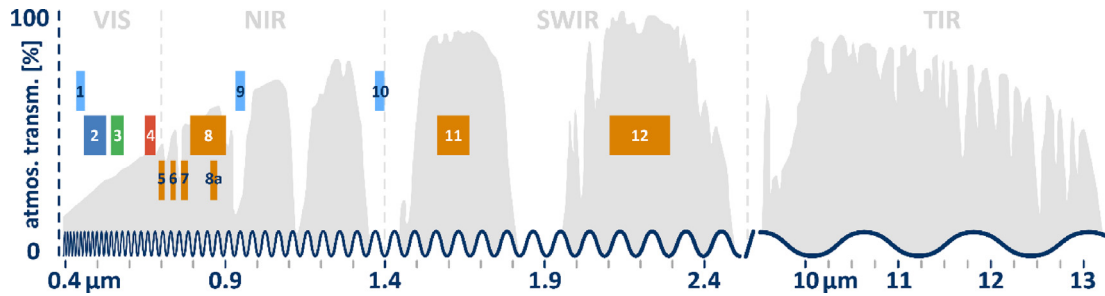


Fig. 15. Sentinel-2 bands [38].

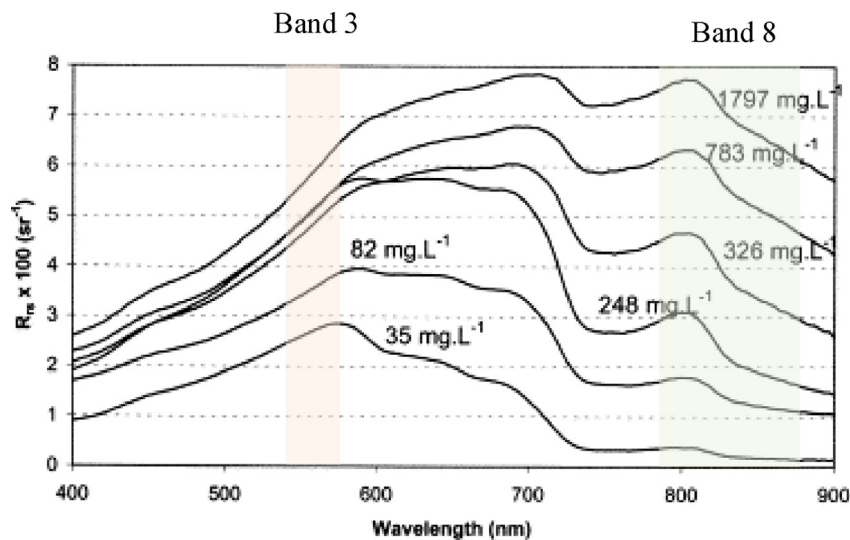


Fig. 16. Spectral signature of highly turbid waters (modified from [39]).

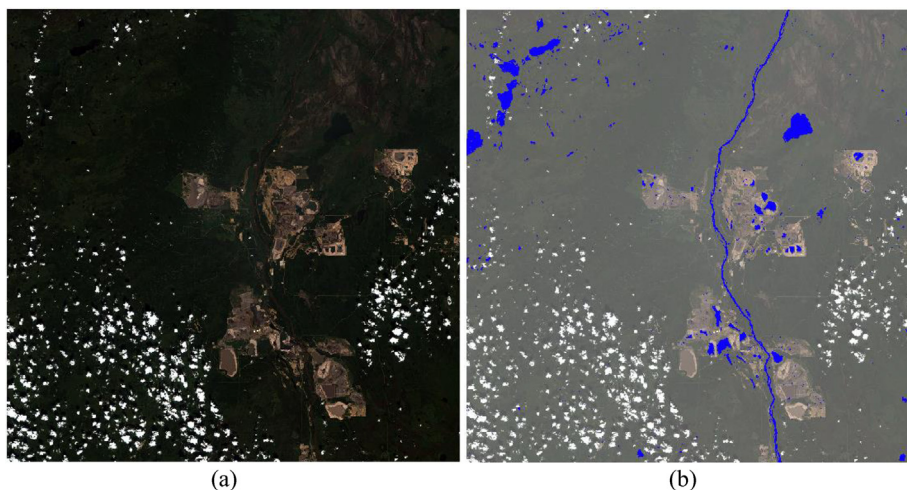


Fig. 17. L2A (BoA) from the year 2017 after atmospheric correction: (a) Without applying NDWI (b) Water flooded areas after NDWI calculation.

and 18, it can be concluded that sections between pixel 375 (point 3) and 550 (point 4) and pixel 725 (point 5) and 1325 (point 6) correspond to water ponds with backscatter reflectance values very close or equal to zero.

On the other hand, Figure 19a shows the whole path of Profile Plot #1 from pixel 0 to pixel 2500. It has Sigma0_VV values in intensity in the range of 0.100 and 0.325, which are typical values for highly vegetated areas. In this plot area, it can be observed that Sentinel-1's radar waves penetrated through the vegetation canopy, and they interacted with the internal structures of the vegetation, such as branches, leaves, and stems. This interaction, known as volume scattering, caused the radar waves to scatter in multiple directions within the vegetation. As a result of this interaction with the vegetation, a significant portion of the radar signal was scattered and, therefore, redirected away from the

radar sensor, leading to low backscattered reflectance and creating dark spots.

Based on the observed patterns and considering various factors that could influence backscatter behavior, such as surface roughness, vegetation density, or liquid bodies, it seems obvious to interpret that possible causes of such dark spots during the observation in 2017 are derived from the presence of shadows occurred when radar signals were blocked or attenuated by dense vegetation as it is shown in Figure 17a. In fact, these objects usually cast shadows, resulting in areas of reduced radar backscatter and appearing as dark spots on the image.

Another important aspect worth mentioning in this study is related to the supervised classification process undertaken with the SAR products. Data obtained (see Table 10) indicates that the classification resulted for the Random Forest process was acceptable for “Forested” and “Oil/Watered” areas

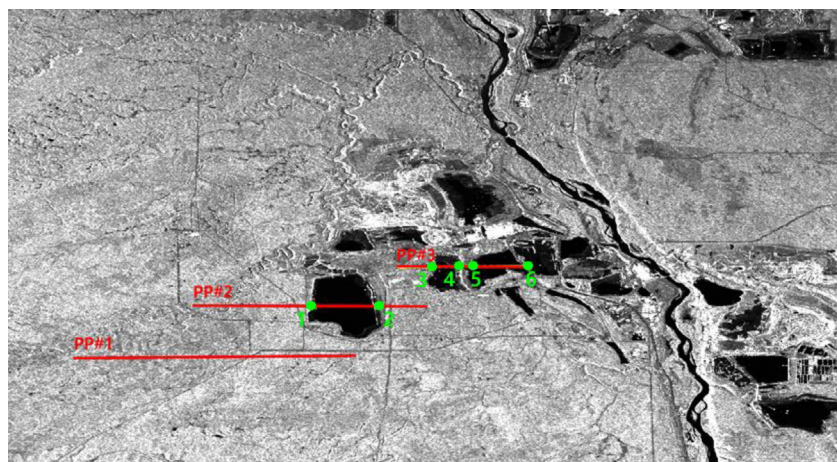


Fig. 18. Location of the profile plots.

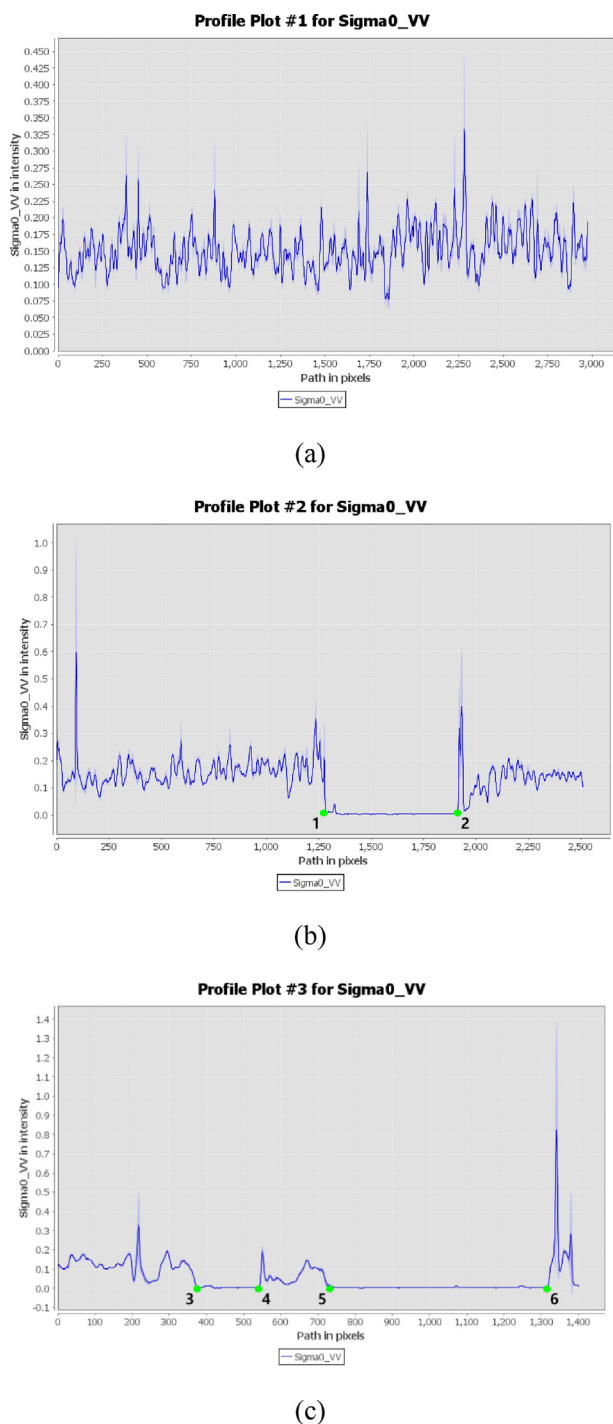


Fig. 19. Sigma0_VV values: (a) Profile Plot #1, (b) Profile Plot #2, (c) Profile Plot #3.

(confidence ranging from 77% to 100%, respectively), but perhaps the “Confidence” was insufficient for “Deforested areas” with values ranging from 52% to 56%. In order to obtain a good classification, it is very important to carry out good training with the dataset. In this sense, a value equal to 500 was used for the variable “Number of trees”

(see Table 7). However, to improve the performance of the supervised classification, other values for the number of trees (up to 5000) and a better selection of pixels used for the training data would be highly recommendable. Some authors [40] suggested that a value of 500 trees could be reasonable for remote sensing studies. Nevertheless, other authors such as [41,42] found it feasible to use a range from 10 up to 5000 trees, depending basically on the spectral-temporal features and the number of features associated with the remote sensing data used for the study.

A second way to likely improve the results during the supervised classification process would be to use a Grey Level Co-occurrence Matrix (GLCM) operator after the “Terrain Correction” during the Batch processing of SAR Products. Since this operator is related to the Textures and could be used to increase the amount of texture information (Contrast, GLMC Mean, and GLMC Variance) in relation to the information content in neighbouring pixels. And also to capture the spatial relationship of pixels in the SAR products. Thus, for land cover classification purposes, texture measures from a GLCM could provide reliable information on the structural distribution and spatial relationship of pixels [43], basically by measuring the probability of obtaining two grey levels, which, in a given direction, can be separated at a given distance.

With respect to the Multispectral analysis carried out in this study, the Normalized Difference Vegetation Index (NDVI) used to check the health and vitality of vegetation was a very effective way to obtain precise information about the amount and vitality of vegetation, therefore, helping to minimize topographic effect and facilitating the differentiation between soil and vegetation areas. Additionally, used combined with MSI Vegetation Analysis of RGB images and the Colour Rough Statistic curves, it provided a useful methodology to easily get a quick approach to a specific study area.

Comparing obtained results with similar studies, it was found that, for instance, David, J., Paull et al. carried out a study in 2006 in which he developed a multi-temporal analysis of the Freeport mining activities using Landsat 5 imagery during the years between 1988 and 2004 [44]. In their research, they used satellite remote sensing to monitor the environmental impact of mining in remote locations, specifically focusing on the PT Freeport Indonesia mine in Papua. The investigation underscored the efficacy of this approach in overseeing the consequences of extensive mining operations and other types of utilization of resources, such as deforestation in developing countries.

In 2010, Elisabeth Schoepfer and Olaf Kranz undertook a study to monitor the exploitation of natural resources, such as mining, using object-based image analysis and GIS [45]. In their study, an object-based multiscale image analysis approach for monitoring natural resources in conflict situations was proposed. The approach used high and very high-resolution optical data to detect the exploitation of natural resources such as mining. They also concluded that object-based image analysis can be used for monitoring natural resource exploitation, emphasizing the idea that the proposed approach allows for efficient and constant monitoring of affected areas.

More recently, in 2018, Jaroslaw Wajs carried out a research study in which he discussed the use of satellite imagery from Sentinel-1A and Sentinel-2A/2B sensors for monitoring mining areas and detecting land changes. He focused on the Belchatow open-cast lignite mine in central Poland [46]. The data analysis methodology utilized in his study was founded on an examination of the remote sensing sensors that were available for ROI analyses. The research was focused on the detection of changes within the Szczerców dumping area in which a careful selection of algorithms, tools, data processing, and spectral classification techniques were used during the research. The processing path for Sentinel-2 and Sentinel-1 data was meticulously elaborated upon. The SLC signal was processed to develop the return intensity map using VV polarization. The resultant SAR image was also reclassified in order to obtain a strong return signal from the open pit and the dumping zone. Their research ultimately determined that the analyzed remote sensing imagery was an effective tool for large-surface analysis, particularly in its ability to detect local anomalies and identify potential hazards. Furthermore, the classification of passive scenes served as an effective means of monitoring land use and change and determining changes in XY components.

In 2021, Narayan Kayet undertook a study using hyperspectral remote sensing techniques for monitoring forest health [47]. The research successfully validated the utility of hyperspectral satellite data in the domain of forest health assessment. Additionally, the study also furnished an efficacious guideline that could be employed for effective forest planning and management. He used two methods for forest health assessment based on the Vegetation indices (VIs) based model and the tree spectral analysis. The supervised classification approach known as Spectral Angle Mapping (SAM) was employed to classify forest health based on spectral information. The findings of the study demonstrated

that healthy areas of the forest were situated mainly on the hilly section of the study zone, while an unhealthy segment was positioned near the mines. The model, which was based on Hyperion data-derived Vegetation Indices (VIs), exhibited superior accuracy compared to other spectral-based methods. Ultimately, the outcomes of the forest health classification were supported by the spectral data of the ground trees. This research provided a valuable guideline for forest management and planning.

The four studies mentioned before were conducted in different years from 2006 to 2021 in the field of remote sensing and environmental monitoring related to mining activities and forest health assessment. Despite addressing different topics and locations, all the studies highlighted the use of satellite remote sensing as an effective tool for monitoring and assessing environmental impacts associated with mining activities and forest health. They emphasized the importance of satellite imagery in monitoring and evaluating the consequences of mining operations, including issues like deforestation and resource exploitation. Furthermore, they highlight the potential and ability of remote sensing to detect land changes and identify potential hazards.

These researches, along with this study on the oilsands, are practical applications which demonstrate how remote sensing works in real-world mining scenarios. Mainly because they provide insights into the efficacy of using satellite data for large-scale analysis, not only identifying local anomalies, monitoring land use and change but also assessing forest health. Moreover, they offer valuable guidelines for effective resource planning and management based on the findings derived from remote sensing techniques.

5. Conclusion

According to the results obtained, Sentinel-2 multispectral bands seem to have a higher practical potential and performance in defining land-covered areas than perhaps the Sentinel-1 backscatter bands. However, SAR images obtained from Sentinel-1 may provide complementary information when Sentinel-2 multispectral images might be affected by clouds, particularly by increasing the separation among classes, especially when it were necessary to process mixed multispectral qualities [48].

On the other hand, there is no way to obtain NDVI values from SAR images, making the use of Sentinel-2 very essential for getting data from the Red and Near Infrared bands.

Analysis performed in this study provides a good example of how the combined use of SAR and Multispectral technologies can be extremely useful in areas affected by bad weather conditions or high cloud coverage. Therefore, the potential of both innovative technologies is improved for monitoring, not only deforestation of mining areas affected by the exploitation of oil sands in Canada but also, the health and vitality of vegetation and other interesting parameters, such as, for instance, water content.

This study comes to prove that SAR and Multispectral analysis of satellite real-time data is a quick and cost-effective method for monitoring deforestation and the good environmental performance of oil sands mining activities, and particularly shows that:

- Total forest and deforested areas for the time period between June 2017 and June 2020 were efficiently measured using data provided by Sentinel-1 and Sentinel-2 satellites.
- Vegetation's health was accurately measured, and the Vegetation Spectral Reflectance Curve in different regions of interest (ROIs) within the surrounding areas close to the mining activities was successfully calculated.
- Accuracy on total forest and deforested areas was obtained from Sentinel-1 and Sentinel-2 satellite data.

For further analysis, it would be interesting to explore the potential of using this satellite technology to analyze how it can contribute to supporting the achievement of the 17 SDGs, the 169 Targets and the 232 Indicators prescribed by the UN Sustainable Development Goals.

Another aspect to be taken into consideration for a deeper search is the possibility of improving the supervised classification process by trying other algorithms as well, not only Random Forest, so that they can contribute to enhancing the performance and confidence of the classified products, also, opening the possibility of making additional comparisons between the supervised classification of SAR products versus Multispectral products in order to study different ways to improve the final results.

The use of Polarimetric SAR interferometry (PolInSAR), which is a technique that uses radar data from synthetic aperture radar (SAR) sensors to estimate the height of forest canopy, could also be considered to be explored in future studies. In fact, since PolInSAR uses the phase difference between horizontally and vertically polarized radar signals to calculate the height of the canopy, it could be a complementary technique to optical systems particularly useful depending on the density of the

forest environment. It could provide high-resolution and accurate estimates of forest height since it has been used in various studies to map and monitor forest canopy height and structure.

Funding body

None.

Conflicts of interest

None declared.

Ethical statement

The authors state that the research was conducted according to ethical standards.

References

- [1] Gibson JJ, Peters DL. Water and environmental management in oil sands regions. *J. Hydrol. Reg. Stud.* 2022;44: 101274. <https://doi.org/10.1016/j.ejrh.2022.101274>.
- [2] Roberts DR, Hazewinkel RO, Arciszewski TJ, Beausoleil D, Davidson CJ, Horb EC, et al. An integrated knowledge synthesis of regional ambient monitoring in Canada's oil sands. *Integr. Environ. Assess. Manag.* 2022;18(2):428–41.
- [3] Asadzadeh S, de Oliveira WJ, de Souza Filho CR. UAV-based remote sensing for the petroleum industry and environmental monitoring: state-of-the-art and perspectives. *J Pet Sci Eng* 2022;208:109633.
- [4] Dubé MG, Dunlop JM, Davidson C, Beausoleil DL, Hazewinkel RRO, Wyatt F. History, overview, and governance of environmental monitoring in the oil sands region of Alberta, Canada. *Integr. Environ. Assess. Manag.* 2022;18(2): 319–32. <https://doi.org/10.1002/ieam.4490>.
- [5] Indarto J, Mutaqin Dadang J. An overview of theoretical and empirical studies on deforestation. *J. Int. Dev. Coop.* 2016; 22(1 & 2):107–20. Retrieved from: https://mpira.ub.uni-muenchen.de/70178/1/JJDC_22-2_107.pdf.
- [6] Lawrence D, Coe M, Walker W, Verchot L, Vandecar K. The unseen effects of deforestation: biophysical effects on climate. *Front. For. Glob. Change* 2022;5. Accessed: Jan. 21, 2023. [Online], <https://www.frontiersin.org/articles/10.3389/ffgc.2022.756115>.
- [7] Kahn J, D'Arcy S, Weis T, Black T. *Line in the tar sands: struggles for environmental justice*. PM Press; 2014.
- [8] Xing R, Chiappori DV, Arbuckle EJ, Binsted MT, Davies EGR. Canadian oil sands extraction and upgrading: a synthesis of the data on energy consumption, CO2 emissions, and supply costs. *Energies* Jan. 2021;14:19. <https://doi.org/10.3390/en14196374>. Art. no. 19.
- [9] Fydrych M. 'Evaluating multi-temporal DInSAR measurements of ground surface deformation around the rhenish coalfields in Germany using sentinel-1 SAR imagery', master thesis. University of Waterloo; 2021. Accessed: Jan. 15, 2023. [Online], <https://uwspace.uwaterloo.ca/handle/10012/17059>.
- [10] Palaniyandi M, Manivel P, Sharmila T, Thirumalai P. The use of multispectral (mss) and synthetic aperture radar (SAR) microwave remote sensing data to study environment variables, land use/land cover changes, and recurrent weather condition for forecast malaria: a systematic review. *Appl Ecol Environ Sci Apr.* 2021;9(4):490–501. <https://doi.org/10.12691/aees-9-4-10>.
- [11] Moreira A, Prats-Iraola P, Younis M, Krieger G, Hajnsek I, Papathanassiou KP. A tutorial on synthetic aperture radar. *IEEE Geosci. Remote Sens. Mag.* Mar. 2013;1(1):6–43. <https://doi.org/10.1109/MGRS.2013.2248301>.

- [12] Landgrebe D. Information extraction principles and methods for multispectral and hyperspectral image data. In: Information processing for remote sensing. World Scientific; 1999. p. 3–37. https://doi.org/10.1142/9789812815705_0001.
- [13] Jing R, Duan F, Lu F, Zhang M, Zhao W. Cloud removal for optical remote sensing imagery using the SPA-CycleGAN network. *J Appl Remote Sens* Aug. 2022;16(3):034520. <https://doi.org/10.1117/1.JRS.16.034520>.
- [14] Li J, Zhang Y, Sheng Q, Wu Z, Wang B, Hu Z, et al. Thin cloud removal fusing full spectral and spatial features for sentinel-2 imagery. *IEEE J. Sel. Top. Appl. Earth Obs. JSTARS*. 2022;15:8759–75. <https://doi.org/10.1109/JSTARS.2022.3211857>.
- [15] Isgró MA, Basallote MD, Caballero I, Barbero L. Comparison of uas and sentinel-2 multispectral imagery for water quality monitoring: a case study for acid mine drainage affected areas (SW Spain). *Remote Sens* 2022;14(16):4053.
- [16] Zhang H, Ma Y, Zhang J, Zhao X, Zhang X, Leng Z. Atmospheric correction model for water–land boundary adjacency effects in landsat-8 multispectral images and its impact on bathymetric remote sensing. *Remote Sens* 2022; 14(19):4769.
- [17] Land cover mapping in cloud-prone tropical areas using sentinel-2 data: integrating spectral features with ndvi temporal dynamics. *Remote Sens Apr*. 2020;12(7):1163. <https://doi.org/10.3390/RS12071163>.
- [18] ‘Development of statistical based decision tree algorithm for mixed class classification with sentinel-2 data’, presented at the international geoscience and remote sensing symposium. *IEEE*; Sep. 2020. p. 2304–7. <https://doi.org/10.1109/IGARSS39084.2020.9324545>.
- [19] Wide-area near-real-time monitoring of tropical forest degradation and deforestation using sentinel-1. *Remote Sens Oct*. 2020;12(19):3263. <https://doi.org/10.3390/RS12193263>.
- [20] Sentinel-1 GRD Preprocessing Workflow Jun. 2019;18(1):11. <https://doi.org/10.3390/ECRS-3-06201>.
- [21] Sentinel-2 data for land cover/use mapping: a review. *Remote Sens Jul*. 2020;12(14):2291. <https://doi.org/10.3390/RS12142291>.
- [22] Reinisch EC, Ziemann A, Flynn EB, Theiler J. Combining multispectral imagery and synthetic aperture radar for detecting deforestation. In: Algorithms, technologies, and applications for multispectral and hyperspectral imagery XXVI. *SPIE*; 2020. p. 72–85.
- [23] Lu M, Hamunyela E. ON-LINE change monitoring with transformed multi-spectral time series, a study case in tropical forest. *Int Arch Photogram Rem Sens Spatial Inf Sci Oct*. 2016;XLI-B7-987–9. <https://doi.org/10.5194/isprs-archives-XLI-B7-987-2016>.
- [24] Lei Y, Treuhart R, Keller M, dos-Santos M, Gonçalves F, Neumann M. Quantification of selective logging in tropical forest with spaceborne SAR interferometry. *Remote Sens Environ Jun*. 2018;211:167–83. <https://doi.org/10.1016/j.rse.2018.04.009>.
- [25] ‘A time-series model for characterizing continuous land cover change’, presented at the International Geoscience and Remote Sensing Symposium. *IEEE*; Jul. 2016. p. 3426–9. <https://doi.org/10.1109/IGARSS.2016.7729885>.
- [26] Estimation of surface roughness over bare agricultural soil from Sentinel-1 data. *Apr*. 2018. Accessed: Jul. 08, 2023. [Online], <https://typeset.io/papers/estimation-of-surface-roughness-over-bare-agricultural-soil-1v01a21rk6>.
- [27] Relation between ERS-1 synthetic aperture radar data and measurements of surface roughness and moisture content of rocky soils in a semiarid rangeland. *Water Resour Res Jun*. 1998;34(6):1491–8. <https://doi.org/10.1029/98WR00032>.
- [28] Integration of L-band derived soil roughness into a bare soil moisture retrieval approach from C-band SAR data. *Remote Sens May* 2021;13(11):2102. <https://doi.org/10.3390/RS13112102>.
- [29] Simultaneously estimating surface soil moisture and roughness of bare soils by combining optical and radar data. *Int. J. Appl. Earth Obs. Geoinformation Aug*. 2021;100: 102345. <https://doi.org/10.1016/J.JAG.2021.102345>.
- [30] Kirsch A, Opeña Disterhoff J, Marr G, Breech R, Louvel Y, Aitken G, et al. Banking on Climate Change. Fossil Fuel Finance Report Card 2017. Rainforest Action Network (RAN) 2017:58. Retrieved from: https://www.ran.org/wp-content/uploads/2018/06/RAN_Banking_On_Climate_Change_2017_final.pdf.
- [31] ‘Alberta Government’. *Government of Alberta open datasets and publications*, Jan. 21, 2023, <https://open.alberta.ca/dataset?q=suncor&sort=score+desc>. accessed Jan. 21, 2023).
- [32] ‘Alberta Energy - Geoview’. Alberta Energy - Geoview, Jan. 21, 2023, <https://gis.energy.gov.ab.ca/Geoview/OSPNG>. accessed Jan. 21, 2023).
- [33] ‘Open Access Hub’. <https://scihub.copernicus.eu/>; Jan. 21, 2023. accessed Jan. 21, 2023).
- [34] User guides - sentinel-1 SAR - sentinel online - sentinel online. <https://sentinels.copernicus.eu/web/sentinel/user-guides/sentinel-1-sar>; Jan. 21, 2023 (accessed Jan. 21, 2023).
- [35] The Sentinel missions - (ESA). https://www.esa.int/Applications/Observing_the_Earth/Copernicus/The_Sentinel_missions; Jan. 21, 2023. accessed Jan. 21, 2023).
- [36] Rouse JW, Haas RH, Schell JA, Deering DW. Monitoring vegetation systems in the great plains with ERTS. *Jan*. 1974. Accessed: Jan. 21, 2023. [Online], <https://ntrs.nasa.gov/citations/19740022614>.
- [37] Gao B. NDWI—a normalized difference water index for remote sensing of vegetation liquid water from space. *Remote Sens Environ Dec*. 1996;58(3):257–66. [https://doi.org/10.1016/S0034-4257\(96\)00067-3](https://doi.org/10.1016/S0034-4257(96)00067-3).
- [38] Sentinel 2. <https://blogs.fu-berlin.de/reseda/sentinel-2/>. accessed Jul. 11, 2023).
- [39] Doxaran D, Froidefond J-M, Lavender S, Castaing P. Spectral signature of highly turbid waters: application with SPOT data to quantify suspended particulate matter concentrations. *Remote Sens Environ Jul*. 2002;81(1):149–61. [https://doi.org/10.1016/S0034-4257\(01\)00341-8](https://doi.org/10.1016/S0034-4257(01)00341-8).
- [40] Belgiu M, Drăguț L. Random forest in remote sensing: a review of applications and future directions. *ISPRS J Photogrammetry Remote Sens Apr*. 2016;114:24–31. <https://doi.org/10.1016/j.isprsjprs.2016.01.011>.
- [41] Du P, Samat A, Waske B, Liu S, Li Z. Random Forest and Rotation Forest for fully polarized SAR image classification using polarimetric and spatial features. *ISPRS J Photogrammetry Remote Sens Jul*. 2015;105:38–53. <https://doi.org/10.1016/j.isprsjprs.2015.03.002>.
- [42] Stumpf A, Kerle N. Object-oriented mapping of landslides using Random Forests. *Remote Sens Environ Oct*. 2011; 115(10):2564–77. <https://doi.org/10.1016/j.rse.2011.05.013>.
- [43] Hall-Beyer M. Practical guidelines for choosing GLCM textures to use in landscape classification tasks over a range of moderate spatial scales. *Int J Rem Sens Mar*. 2017;38(5): 1312–38. <https://doi.org/10.1080/01431161.2016.1278314>.
- [44] Monitoring the environmental impact of mining in remote locations through remotely sensed data. *Geocarto Int Mar*. 2006;21(1):33–42. <https://doi.org/10.1080/10106040608542372>.
- [45] Monitoring natural resources in conflict using an object-based multiscale image analysis approach. *Jun*. 2010. Accessed: Jul. 10, 2023. [Online], <https://typeset.io/papers/monitoring-natural-resources-in-conflict-using-an-object-1svzoa55a0>.
- [46] First experience with Remote Sensing methods and selected sensors in the monitoring of mining areas – a case study of the Belchatow open cast mine Jan. 2018;vol. 29:00023. <https://doi.org/10.1051/E3SCONF/20182900023>.
- [47] Forest health monitoring using hyperspectral remote sensing techniques. *Jan*. 2021. p. 239–57. https://doi.org/10.1007/978-3-030-56542-8_10.
- [48] Aaron M. “An Evaluation of Sentinel-1 and Sentinel-2 for Land Cover Classification”. International Development, Community and Environment (IDCE) 2019. 235. Retrieved from: https://commons.clarku.edu/idce_masters_papers/235.